Targeting miR-423-5p Reverses Exercise Training-Induced HCN4 Channel Remodeling and Sinus Bradycardia

Alicia D'Souza[1], Charles M Pearman[1], Yanwen Wang[1], Shu Nakao[1], Sunil Jit RJ Logantha[1], Charlotte Cox[1], Hayley Bennett[1], Yu Zhang[1], Anne Berit Johnsen[2], Nora Linscheid[3], Pi Camilla Poulsen[3], Jonathan Elliott[1], Jessica Coulson[4], Jamie McPhee[4], Abigail Robertson[1], Paula Da Costa Martins[5], Ashraf Kitmitto[1], Ulrik Wisloff[2,6], Elizabeth J. Cartwright[1], Oliver Monfredi[1], Alicia Lundby[3], Halina Dobrzynski[1], Delvac Oceandy[1], Gwilym M. Morris[1], Mark R. Boyett[1]

A.D'S, C.M.P., and Y.W. contributed equally to this manuscript.

H.D., D.O., G.M.M., and M.R.B share senior authorship.

[1]University of Manchester, United Kingdom; [2]Norwegian University of Science and Technology, Norway; [3]University of Copenhagen, Denmark; [4]Manchester Metropolitan University, UK; [5]Maastricht University, Netherlands, and; [6]University of Queensland, Australia.

Running title: miR-423-5p Causes Training-Induced Bradycardia

Subject Terms:
Arrhythmias
 Electrophysiology
Exercise
Ion Channels/Membrane Transport
Mechanisms

Address correspondence to:
Dr. Mark Boyett
Division of Cardiovascular Sciences
46 Grafton Street
Manchester M13 9NT, UK
Tel: +44-161-2751192
mark.boyett@manchester.ac.uk

In July 2017, the average time from submission to first decision for all original research papers submitted to *Circulation Research* **was 12.8 days**

ABSTRACT

***Rationale*:** Downregulation of the pacemaking ion channel, HCN4, and the corresponding ionic current, I_f, underlies exercise training-induced sinus bradycardia in rodents. If this occurs in humans, it could explain the increased incidence of bradyarrhythmias in veteran athletes and it will be important to understand the underlying processes.

***Objective*:** To test the role of HCN4 in the training-induced bradycardia in human athletes and investigate the role of micro-RNAs (miRs) in the repression of HCN4.

***Methods and Results*:** As in rodents, the intrinsic heart rate was significantly lower in human athletes than non-athletes and in all subjects the rate-lowering effect of the HCN selective blocker, ivabradine, was significantly correlated with the intrinsic heart rate, consistent with HCN repression in athletes. Next generation sequencing and qPCR showed remodelling of miRs in the sinus node of swim-trained mice. Computational predictions highlighted a prominent role for miR-423-5p. Interaction between miR-423-5p and HCN4 was confirmed by a dose-dependent reduction in HCN4 3′-UTR luciferase reporter activity on co-transfection with precursor miR-423-5p (abolished by mutation of predicted recognition elements). Knockdown of miR-423-5p with antimiR-423-5p reversed training-induced bradycardia via rescue of HCN4 and I_f. Further experiments showed that, in the sinus node of swim-trained mice, upregulation of miR-423-5p (intronic miR) and its host gene, NSRP1, is driven by an upregulation of the transcription factor Nkx2.5.

Conclusions: HCN remodelling likely occurs in human athletes as well as rodent models. miR-423-5p contributes to training-induced bradycardia by targeting HCN4. This work presents the first evidence of miR control of HCN4 and heart rate. miR-423-5p could be a therapeutic target for pathological sinus node dysfunction in veteran athletes.

Keywords:
Athletes, sinus bradycardia, ion channel remodelling, micro-RNAs, exercise training, sinoatrial node.

Nonstandard Abbreviations and Acronyms:

HCN4	hyperpolarization-activated cyclic nucleotide gated channel 4
I_f	funny current
FDR	false discovery rate
micro-RNA	miR – microribonucleic acid
qPCR	quantitative real-time reverse transcription polymerase chain reaction
UTR	untranslated region

INTRODUCTION

Athletes are prone to cardiac arrhythmias and sinus bradycardia is the most common rhythm 'disturbance'.[1] In the long term, this physiological adaptation can become pathological as veteran athletes are more likely to have sinus node dysfunction and to need an electronic pacemaker implantation than non-athletes.[2-4] In two rodent models of exercise training, we previously demonstrated that the training-induced bradycardia is predominantly the result of a downregulation of the key pacemaking ion channel HCN4 and the corresponding ionic current (funny current, I_f) in the sinus node.[5] We now report the first evidence that HCN4 and I_f downregulation is also responsible for training-induced sinus bradycardia in human athletes. What is responsible for the downregulation of HCN4 in the athlete? Despite its fundamental importance, regulation of HCN4 in health and disease is poorly understood. micro-RNAs (miRs) have been shown to play pivotal roles in cardiac remodelling in a variety of settings by post-transcriptional silencing of genes.[6-9] Some miRs have been implicated in ion channel remodelling.[7-9] We report here that the downregulation of HCN4 and I_f in trained mice is the result of an upregulation of miR-423-5p in the sinus node and the training-induced bradycardia can be reversed by targeting the miR-dependent HCN4 remodelling.

METHODS

A 3-lead ECG was recorded from male volunteers aged 18-30 years: 8 competitive endurance athletes and 10 sedentary age-matched (control) subjects. The heart rate was measured before and after complete autonomic blockade (achieved by intravenous injection of 0.04 mg/kg atropine and 0.2 mg/kg propranolol followed by top-up doses). After complete autonomic blockade, 7.5 mg ivabradine was administered orally and the change in heart rate recorded and used as a measure of the involvement of I_f in pacemaking. 10-week-old C57BL/6J mice were trained by swimming for 60 min twice daily for 28 days.[5] miR, mRNA and protein expression in sinus node biopsies was measured by next generation sequencing, quantitative PCR (qPCR), western blot and high-resolution mass spectrometry. Computational predictions, luciferase reporter gene assays and in vitro overexpression studies were used to identify miRs and transcription factors capable of regulating expression. The role of a candidate miR in the training-induced bradycardia was tested in vivo by administering an appropriate cholesterol-conjugated antimiR.[6] ECG recording, in vitro tissue electrophysiology, western blot, sinus node cell isolation and whole cell patch clamp were used to characterise the mice and study HCN4 and I_f remodelling. Statistically significant differences were determined using an appropriate test; $P<0.05$ was regarded as significant. In figures, bar charts show means±SEM. Further details of methods are available in the Online Data Supplement.

RESULTS

Evidence of I_f remodelling in human athletes.

Experiments were conducted on groups of human male non-athletes (n=10) and athletes (n=8). The characteristics of the two groups are given in Online Table I. As expected, the maximum O_2 uptake (VO$_2$max, a measure of fitness) of the athletes was significantly higher than that of the non-athletes (Fig. 1A). Figure 1B shows the resting heart rate under baseline conditions of the two groups of subjects; as expected the heart rate of the athletes was significantly lower. It is still widely thought that the training-induced bradycardia is the result of an increase in vagal tone based on reported increases in heart rate variability in athletes;[e.g.10] heart rate variability is considered a measure of autonomic tone. However, we have recently shown that heart rate variability is primarily determined by heart rate and not autonomic tone.[11] In the present study, neither uncorrected SDNN (standard deviation of normal to normal beats, a

measure of heart rate variability) or SDNN corrected for changes in heart rate[11] was increased in the athletes (Online Table I). Figure 1B also shows the intrinsic heart rate after complete autonomic blockade in the two groups of subjects. Autonomic blockade was achieved by intravenous injection of 0.2 mg/kg propranolol and 0.04 mg/kg atropine, doses which have previously been demonstrated to cause complete autonomic blockade in human subjects.[12, 13] The intrinsic heart rate after complete autonomic blockade in the non-athletes was 97.9±2.6 beats/min, similar to the value reported by Jose and Collison[14] of 105.6±0.6 beats/min from 139 untrained male subjects 20-30 years of age. This suggests that complete autonomic blockade was achieved (see Online Data Supplement for further discussion).[15] Furthermore, heart rate variability was almost completely eliminated after autonomic blockade: uncorrected SDNN was reduced by 94%, corrected SDNN was reduced by 90% and high frequency spectral heart rate variability was reduced by >99% (Figure 1C). This is consistent with complete autonomic blockade. Figure 1B shows that there was a significant bradycardia in the athletes (as compared to the non-athletes) after complete autonomic blockade as well as under baseline conditions (the relative bradycardia was *larger* after complete autonomic blockade). We conclude that the bradycardia cannot be attributed to the autonomic nervous system, although we appreciate that others have concluded that it is the result of high vagal tone (see Online Data Supplement for further discussion). Figure 1D shows that the intrinsic heart rate of the non-athletes and athletes is significantly correlated with the fitness of the subjects as measured by the VO_2max). Figure 1E shows a significant correlation between the heart rate lowering effect of oral ivabradine (blocks HCN4 and I_f) and the intrinsic heart rate of the non-athletes and athletes: subjects with a lower intrinsic heart rate (generally athletes) had a blunted response to ivabradine. This suggests that in the human athlete there is a downregulation of HCN4 and I_f and this could be the cause (or at least a key contributing cause) of the training-induced bradycardia.

Training-induced downregulation of HCN4 and dysregulation of miRs.

Following swim-training for four weeks in the mouse, there was a significant bradycardia both in vivo and in the isolated sinus node (Figure 2A). This was confirmed by intracellular action potential recording from the isolated sinus node; the bradycardia was accompanied by a small positive shift of the maximum diastolic potential and prolongation of the action potential (Online Table II). The two main pacemaking mechanisms are the membrane and Ca^{2+} clocks.[16] Whereas the main Ca^{2+} clock transcripts in the sinus node were unaffected by training (Online Figure I), the transcript for HCN4 (the main component of the membrane clock[16]) was significantly downregulated in the sinus node after training (Figure 2B). As expected this was accompanied by a reduction of I_f over a wide potential range in isolated sinus node cells from trained mice (Figure 2C). Consistent with this, Figure 2D shows that, in the mouse as in the human (Figure 1E), there is a significant correlation between the heart rate lowering effect of ivabradine and the intrinsic heart rate: mice with a lower intrinsic heart rate (generally trained) had a blunted response to ivabradine. These data are consistent with a downregulation of HCN4 and I_f being the cause of the training-induced bradycardia in mice, consistent with our previous study.[5]

In sinus node biopsies, we measured expression of all miRs using next generation sequencing. 715 microRNAs were detected in the sinus node. DeSeq analysis showed 25 miRs were significantly increased >1.8 fold and 6 significantly decreased (Figure 2E; Online Table III). After applying a 5% Benjamini-Hochberg false discovery rate correction, miR-5099, miR-486-3p, miR-423-5p, Let-7d-3p, miR-676-3p, miR-181b-5p and Let-7e-5p were significantly upregulated and miR-10b-5p downregulated (Figure 2E, hatched bars). qPCR analysis confirmed the majority of these changes (including in miR-423-5p; Figure 2F).

HCN4 is target gene for miR-423-5p.

A computational search was conducted (see Online Data Supplement) to establish a link between significantly upregulated miRs and HCN4 downregulation. miRs bind cognate mRNAs by imprecise

complementary base pairing to specific sequence motifs primarily in the 3′-UTR.[17] Using the widely employed algorithms RNA22,[18] PITA[19] and TargetScan Mouse v7.1,[20] we identified putative recognition sites for miR-423-5p (Online Figure II) and miR-486-3p (data not shown) within the mouse HCN4 3′-UTR sequence. To verify these predicted binding sites and experimentally establish HCN4 as a genuine target, we fused the HCN4 3′-UTR to a luciferase reporter gene (pHCN4-3′ UTR) and determined luciferase activity in H9c2 cells co-transfected with pHCN4-3′ UTR and synthetic precursors to miR-423-5p and miR-486-3p. Additionally, we included miR-1 and miR-27a in this analysis as we have previously found miR-1 to be upregulated in the sinus node of the trained mouse and rat[5] and all computational tools used indicated the presence of a highly conserved binding site for miR-27a. All miRs tested significantly supressed luciferase activity relative to a control (scrambled) miR, although suppression was modest on transfection with miR-1 and miR-486-3p (34%; data not shown) compared to miR-423-5p (Figure 3A). Surprisingly, miR-27a only produced a small suppression of luciferase activity (Figure 3A).

We selected miR-423-5p for further study, because it was predicted to target HCN4, it was significantly upregulated using both next generation sequencing (2.8-fold increase above baseline) and qPCR (8.1-fold increase above baseline) and it produced the largest suppression of luciferase activity amongst the miRs tested. We observed a dose-dependent effect of miR-423-5p on luciferase activity of pHCN4-3′ UTR (Figure 3C). Furthermore, mutation of predicted miR-423-5p binding sequences in the HCN4 3′- UTR (Figure 3B) abolished the effect of miR-423-5p on reporter expression (Figure 3C). These findings demonstrate a specific interaction between miR-423-5p and HCN4 and the predicted recognition elements identified in the HCN4 3′-UTR contribute to this. Both HCN4 mRNA and intrinsic heart rate showed a significant inverse correlation with expression of miR-423-5p (Figure 3D,E). Linear regression analysis showed that the sinus node expression level of miR-423-5p explained 68% of the variation in HCN4 (Figure 3D; $R^2=0.68$) and 46% of the variation in spontaneous beating rate of the sinus node (Figure 3E; $R^2=0.46$). Upregulation of miR-423-5p appeared to be restricted to the trained sinus node – basal expression of miR-423-5p was lower in the atrium and ventricle and was unaltered by training (Figure 3F). Following two weeks of detraining (after four weeks of training), there was a partial restoration of miR-423-5p (Figure 3G).

Although Figure 3A-C shows that miR-423-5p targets HCN4, it is possible that it has other targets. Previously, miR-423-5p has been reported to cause apoptosis of cardiomyocytes[21-23] and we performed the TUNEL assay to assess apoptosis. However, we observed very few apoptotic cells in the sinus node and there was no significant difference in the number in sedentary and trained mice (Online Figure III).

Training-induced downregulation of HCN4 and I_f and resulting sinus bradycardia is result of upregulation of miR-423-5p.

We hypothesised that the training-induced upregulation of miR-423-5p results in the downregulation of HCN4 and consequently a lower heart rate. To test this, miR-423-5p was knocked down in vivo via three daily intraperitoneal injections of cholesterol-conjugated anti-miR-423-5p (antimiR) in sedentary mice and in trained mice at day 25-27 of the swimming protocol (Figure 4A). Administered in this way, cholesterol-conjugated antimiR has previously been documented to be highly effective in knocking down target miR in the heart with long-lasting efficacy under in vivo conditions.[6] At day 28, i.e. 3 days after the first administration, qPCR analysis showed a dramatic reduction in the level of miR-423-5p (Figure 4B). A separate study demonstrated that the suppressive effect of the antimiR on miR-423-5p persisted for up to 3 weeks after administration (Online Figure IV). Remarkably, the antimiR abolished or blunted the training-induced bradycardia: it restored the heart rate measured in vivo and in vitro (isolated sinus node) to or towards the pre-training level (Figure 4C). Intriguingly, the antimiR did not alter the heart rate in vivo in sedentary animals despite successful knockdown of miR-423-5p (Online Figure V); the effect of the antimiR was therefore restricted to the trained mouse. Western blot analysis demonstrated that the

antimiR completely restored total HCN4 protein in the sinus node (level in antimiR-treated mice was 2.1× greater than that in vehicle-treated sedentary mice; Figure 4D). The effect of antimiR on I_f was assessed in vitro by pharmacological block of I_f with 2 mM Cs^+ in the isolated sinus node (Figure 4E).[24] 2 mM Cs^+ produced a smaller decrease in spontaneous beating rate in trained animals (indicative of reduction in I_f) and this effect was reversed by the antimiR, indicating restoration of I_f by the antimiR (Figure 4E). Whole cell patch clamp recordings from isolated sinus node cells confirmed this: the density of I_f was reduced in trained mice and it was almost fully restored in trained mice treated with the antimiR (Figure 4F). In summary, the antimiR restored total HCN4 protein (transmembrane fraction of which is responsible for I_f) beyond the control level, almost fully restored I_f, fully restored responsiveness to Cs^+ (indirect measure of I_f), almost fully restored the intrinsic heart rate (arguably set by I_f) measured in the isolated sinus node, and fully restored the heart rate measured in vivo (again arguably set by I_f). Total HCN4 protein may have been restored beyond the control level, because of an increase in the amount of protein being trafficked to the membrane. It is not known why heart rate in vivo was fully restored whereas I_f was only partially restored – it is possible that there is an additional mechanism in operation. A control (non-targeting) antimiR did not restore I_f (Online Figure VI). The heart weight:body weight ratio and various ECG parameters were largely unaffected by the antimiR (Online Figure VII).

Control of miR-423-5p in the trained sinus node.

miR-423 is located in the first intron of its host gene, NSRP1, and both are transcribed in the same 'sense' direction (Figure 5A). Therefore, it is possible that they are co-regulated and share regulatory (promoter) elements, as has been shown previously for intronic miRs.[25, 26] qPCR confirmed that NSRP1 mRNA was significantly upregulated in the sinus node of trained mice (Figure 5B). A bioinformatics search using MatInspector revealed transcription factors that could potentially bind to the promoter region of NSRP1. The expression of the 88 top predicted transcription factors in the sinus node was investigated using qPCR – 15 were significantly upregulated and two significantly downregulated following training (Figure 5C). Of these 17, Nkx2.5 (data for Nkx2.5 shown in more detail in Figure 5D) was the most promising on the basis it was upregulated (therefore, potentially explaining the upregulation of NSRP1), it is an important cardiac transcription factor, it is known to work in consort with other transcription factors (Foxp1, Stat3 and Tbx5[27-29]) that were also upregulated in the sinus node with athletic training (Fig. 5C), it represses the working phenotype in the sinus node, and most importantly it has previously been shown that upregulation is associated with 'sick sinus disease' and sinus bradycardia.[30] Although Nkx2.5 is thought not to be expressed in the adult sinus node, we observed substantial expression of both Nkx2.5 mRNA and protein in the sinus node even in the case of the sedentary mouse (Online Figure X; see Online Data Supplement for further discussion). Predicted Nkx2.5 binding sites on NSRP1 are given in Online Figure VIII. To verify NSRP1 as a target of Nkx2.5, we fused 2.1 kb of the 5′ flanking region of NSRP1 (upstream of the transcriptional start site) to luciferase and determined luciferase activity in H9c2 cells co-transfected with an Nkx2.5 overexpression plasmid. Nkx2.5 significantly increased luciferase activity relative to vehicle control (Figure 5E). To confirm this finding, Nkx2.5 was then overexpressed in H9c2 cells. Surprisingly Nkx2.5 had little effect on expression of NSRP1 (Online Figure IX), but it resulted in a robust increase in miR-423-5p (Fig. 5F). It is possible that miR-423-5p is one of 20% of intronic miRs that are predicted to inhibit expression of their host gene.[31] In this case, whether Nkx2.5 upregulates both NSRP1 and miR-423-5p may depend on the precise circumstances. We conclude from these data that the upregulation of miR-423-5p in the sinus node following training involves an upregulation of the transcription factor, Nkx2.5.

DISCUSSION

Our previous work on rodents was the first to attribute exercise training-induced bradycardia to the downregulation of HCN4 and I_f.[5] We now present evidence suggesting this is also the case in human athletes. In addition, we show that HCN4 is a novel target for post-transcriptional repression by miR-423-5p and the training-induced downregulation of HCN4 and I_f and consequently the bradycardia is the result of an upregulation of Nkx2.5 and consequently miR-423-5p in the sinus node. This is the first report of miR-dependent regulation of pacemaking and heart rate.

There is widespread belief that the resting bradycardia in athletes is the result of high vagal tone, although vagal tone has never been directly measured in athletes.[e.g.32] However, critical analysis of the literature does not necessarily support this.[15, 33, 34] An increase in heart rate variability in human athletes has been extensively quoted as evidence for high vagal tone in athletes.[e.g.32] However, we have shown from an analysis of the underlying biophysics of pacemaking that heart rate variability is primarily determined (in an exponential-like manner) by heart rate and the increase in heart rate variability in athletes is attributed to the resting bradycardia rather than any increase in vagal tone.[11] This study has shown that the relative bradycardia in human athletes (as compared to the heart rate of the control subjects) was still present (and in fact was larger) after complete autonomic blockade (Figure 1B). The same result (a larger relative bradycardia after autonomic blockade) has been reported by three other studies of human athletes.[15] This suggests that the autonomic nervous system is not responsible for the resting bradycardia. Once again, many studies of animal models of exercise training show no evidence of high vagal tone.[15] However, some studies of human athletes or animal models of exercise training apparently show a reduction of the relative bradycardia after autonomic blockade, leaving open the possibility that high vagal tone does play a role.[15, 35, 36] This is considered further in the Supplementary Discussion. Previously, we showed that the reduction of heart rate on blocking I_f by ivabradine or Cs^+ is decreased in the trained rodent and this is attributed to the training-induced downregulation of HCN4 and I_f.[5] The corollary of this, as shown in Figure 2D, is that there is a correlation between the effect of ivabradine and the intrinsic heart rate of sedentary and trained mice. As shown in Figure 1E, the same correlation is observed in sedentary and trained human subjects. It is, therefore, possible that there is a training-induced downregulation of HCN4 and I_f in the human athlete and this is the cause (or at least a contributing cause) of the bradycardia.

miR profiling by next generation sequencing revealed 35 miRs to be altered by endurance training in the sinus node (Figure 2E). Several of these miRs have previously been shown to exert regulatory effects in the heart: miR-486-3p, upregulated in the sinus node of the trained mice (Figure 2E,F), has previously been shown to be upregulated in the hearts of swim-trained mice and involved in the anti-fibrotic effects of exercise;[37] Let-7e, upregulated in the sinus node of the trained mice (Figure 2E,F), has previously been shown to have an anti-arrhythmic effect mediated via a downregulation of the β1 adrenergic receptor in myocardial infarction rats;[38] finally, miR-10b-5p, downregulated in the sinus node of the trained mice (Figure 2E,F), has previously been shown to regulate the key cardiac transcription factor Tbx5, known to be involved with the cardiac conduction system.[39] Previously, the plasma level of miR-423-5p has been reported to be elevated in heart failure, acute myocardial infarction, stable coronary artery disease and patients undergoing cardiac surgery.[40-42] In the case of heart failure at least, this is thought to be the result of altered myocardial expression.[42] In these studies, although the source of miR-423-5p may be the myocardium, it is not known from what part of the heart it originates. Figure 3F suggests that miR-423-5p is preferentially expressed by the sinus node and this raises the question of whether the sinus node is the source of miR-423-5p in heart failure etc. Paradoxically, the sinus node in heart failure is like that in the athlete; there is intrinsic sinus bradycardia and a widespread remodelling of the sinus node with a downregulation of ion channels.[e.g.43-45] miRs are known to function according to a 'combinatorial circuitry model', whereby a single miR targets multiple mRNAs and several co-expressed miRs may target a single mRNA.[46] While our data suggests a prominent role for miR-423-5p in regulating HCN4, we cannot rule

out a role for other miRs. Ultimately, regulation of heart rate is a complex and dynamic process involving acute regulation by the autonomic nervous system and longer-term regulation involving changes in ion channel expression brought about by transcription factors and, as shown for the first time by our study, miRs.

In conclusion, our findings provide new insight into the molecular mechanisms underlying the sinus bradycardia in athletes and this may have implications for other conditions in which I_f is dysregulated, e.g. heart failure.[43] Although the changes in the sinus node and sinus bradycardia are well tolerated by healthy young athletes, this is not necessarily the case in some veteran athletes and the changes manifest as pathological sinus node dysfunction - the incidence of pacemaker implantation in veteran athletes is higher than in non-athletes.[2-4] Inhibition of miR-423-5p (especially because upregulation of miR-423-5p could be restricted to the sinus node – Figure 3F) could be an alternative therapeutic strategy to electronic pacemaker implantation for pathological sinus node dysfunction seen in some veteran athletes.

DISCLOSURES
None.

REFERENCES

1.   Link MS, Homoud MK, Wang PJ and Estes NA, 3rd. Cardiac arrhythmias in the athlete: the evolving role of electrophysiology. *Current Sports Medicine Reports*. 2002;1:75-85.

2.   Northcote RJ, Canning GP and Ballantyne D. Electrocardiographic findings in male veteran endurance athletes. *British Heart Journal*. 1989;61:155-60.

3.   Northcote RJ, Rankin AC, Scullion R and Logan W. Is severe bradycardia in veteran athletes an indication for a permanent pacemaker? *British Medical Journal*. 1989;298:231-2.

4.   Baldesberger S, Bauersfeld U, Candinas R, Seifert B, Zuber M, Ritter M, Jenni R, Oechslin E, Luthi P, Scharf C, Marti B and Attenhofer Jost CH. Sinus node disease and arrhythmias in the long-term follow-up of former professional cyclists. *European Heart Journal*. 2008;29:71-78.

5.   D'Souza A, Bucchi A, Johnsen AB, Logantha SJ, Monfredi O, Yanni J, Prehar S, Hart G, Cartwright E, Wisloff U, Dobryznski H, DiFrancesco D, Morris GM and Boyett MR. Exercise training reduces resting heart rate via downregulation of the funny channel HCN4. *Nature Communications*. 2014;5:3775.

6.   Dirkx E, Gladka MM, Philippen LE, Armand AS, Kinet V, Leptidis S, El Azzouzi H, Salic K, Bourajjaj M, da Silva GJ, Olieslagers S, van der Nagel R, de Weger R, Bitsch N, Kisters N, Seyen S, Morikawa Y, Chanoine C, Heymans S, Volders PG, Thum T, Dimmeler S, Cserjesi P, Eschenhagen T, da Costa Martins PA and De Windt LJ. Nfat and miR-25 cooperate to reactivate the transcription factor Hand2 in heart failure. *Nature Cell Biology*. 2013;15:1282-93.

7.   Yang B, Lin H, Xiao J, Lu Y, Luo X, Li B, Zhang Y, Xu C, Bai Y, Wang H, Chen G and Wang Z. The muscle-specific microRNA miR-1 regulates cardiac arrhythmogenic potential by targeting GJA1 and KCNJ2. *Nature Medicine*. 2007;13:486-91.

8.   Lu Y, Zhang Y, Wang N, Pan Z, Gao X, Zhang F, Shan H, Luo X, Bai Y, Sun L, Song W, Xu C, Wang Z and Yang B. MicroRNA-328 contributes to adverse electrical remodeling in atrial fibrillation. *Circulation*. 2010;122:2378-87.

9.   Girmatsion Z, Biliczki P, Bonauer A, Wimmer-Greinecker G, Scherer M, Moritz A, Bukowska A, Goette A, Nattel S, Hohnloser SH and Ehrlich JR. Changes in microRNA-1 expression and IK1 up-regulation in human atrial fibrillation. *Heart Rhythm*. 2009;6:1802-9.

10.   Coote JH and White MJ. CrossTalk proposal: bradycardia in the trained athlete is attributable to high vagal tone. *Journal of Physiology*. 2015;593:1745-7.

11.   Monfredi O, Lyashkov AE, Johnsen AB, Inada S, Schneider H, Wang R, Nirmalan M, Wisloff U, Maltsev VA, Lakatta EG, Zhang H and Boyett MR. Biophysical characterisation of the under-appreciated and important relationship between heart rate variability and heart rate. *Hypertension*. 2014;64:1334-1343.

12.   Jose AD and Taylor RR. Autonomic blockade by propranolol and atropine to study intrinsic myocardial function in man. *Journal of Clinical Investigation*. 1969;48:2019-2031.

13.   Katona PG, McLean M, Dighton DH and Guz A. Sympathetic and parasympathetic cardiac control in athletes and nonathletes at rest. *Journal of Applied Physiology*. 1982;52:1652-1657.

14.   Jose AD and Collison D. The normal range and determinants of the intrinsic heart rate in man. *Cardiovascular Research*. 1970;4:160-167.

15.   Boyett MR, D'Souza A, Zhang H, Morris GM, Dobrzynski H and Monfredi O. Viewpoint: Is the resting bradycardia in athletes the result of remodelling of the sinoatrial node rather than high vagal tone? *Journal of Applied Physiology*. 2013;114:1351-1355.

16.   Dobrzynski H, Anderson RH, Atkinson A, Borbas Z, D'Souza A, Fraser JF, Inada S, Logantha SJRJ, Monfredi O, Morris GM, Moorman AFM, Nikolaidou T, Schneider H, Szuts V, Temple IP, Yanni J and Boyett MR. Structure, function and clinical relevance of the cardiac conduction system, including the atrioventricular ring and outflow tract tissues. *Pharmacology & Therapeutics*. 2013;139:260-288.

17.   Filipowicz W, Bhattacharyya SN and Sonenberg N. Mechanisms of post-transcriptional regulation by microRNAs: are the answers in sight? *Nature Reviews Genetics*. 2008;9:102-14.

18.   Miranda KC, Huynh T, Tay Y, Ang YS, Tam WL, Thomson AM, Lim B and Rigoutsos I. A pattern-based method for the identification of microRNA binding sites and their corresponding heteroduplexes. *Cell*. 2006;126:1203-17.

19.   Kertesz M, Iovino N, Unnerstall U, Gaul U and Segal E. The role of site accessibility in microRNA target recognition. *Nat Genet*. 2007;39:1278-84.

20.   Agarwal V, Bell GW, Nam JW and Bartel DP. Predicting effective microRNA target sites in mammalian mRNAs. *eLife*. 2015;4.

21.   Luo P, He T, Jiang RJ and Li G. MicroRNA-423-5p targets O-GlcNAc transferase to induce apoptosis in cardiomyocytes. *Mol Med Rep*. 2015;12:1163-1168.

22.   Li QX, Yu Q, Na RM and Liu BT. MiR-423-5p inhibits human cardiomyoblast proliferation and induces cell apoptosis by targeting Gab 1. *Int J Clin Exp Patho*. 2016;9:8953-8962.

23.   Luo P and Zhang W. MicroRNA-423-5p mediates H_2O_2-induced apoptosis in cardiomyocytes through O-GlcNAc transferase. *Mol Med Rep*. 2016;14:857-864.

24.   Nikmaram MR, Boyett MR, Kodama I, Suzuki R and Honjo H. Variation in the effects of Cs^+, UL-FS 49 and ZD7288 within the sinoatrial node. *American Journal of Physiology*. 1997;272:H2782-H2792.

25.   Baskerville S and Bartel DP. Microarray profiling of microRNAs reveals frequent coexpression with neighboring miRNAs and host genes. *RNA*. 2005;11:241-7.

26.   Kim YK and Kim VN. Processing of intronic microRNAs. *EMBO Journal*. 2007;26:775-83.

27.   Hiroi Y, Kudoh S, Monzen K, Ikeda Y, Yazaki Y, Nagai R and Komuro I. Tbx5 associates with Nkx2-5 and synergistically promotes cardiomyocyte differentiation. *Nat Genet*. 2001;28:276-80.

28.   Zhang Y, Li S, Yuan L, Tian Y, Weidenfeld J, Yang J, Liu F, Chokas AL and Morrisey EE. Foxp1 coordinates cardiomyocyte proliferation through both cell-autonomous and nonautonomous mechanisms. *Genes & Development*. 2010;24:1746-57.

29.   Snyder M, Huang XY and Zhang JJ. Stat3 directly controls the expression of Tbx5, Nkx2.5, and GATA4 and is essential for cardiomyocyte differentiation of P19CL6 cells. *Journal of Biological Chemistry*. 2010;285:23639-46.

30.   Wu M, Peng S, Yang J, Tu Z, Cai X, Cai CL, Wang Z and Zhao Y. Baf250a orchestrates an epigenetic pathway to repress the Nkx2.5-directed contractile cardiomyocyte program in the sinoatrial node. *Cell Research*. 2014;24:1201-13.

31.   Gao X, Qiao Y, Han D, Zhang Y and Ma N. Enemy or partner: relationship between intronic micrornas and their host genes. *IUBMB Life*. 2012;64:835-40.

32.   Billman GE, Cagnoli KL, Csepe T, Li N, Wright P, Mohler PJ and Fedorov VV. Exercise training-induced bradycardia: evidence for enhanced parasympathetic regulation without changes in intrinsic sinoatrial node function. *Journal of Applied Physiology*. 2015;118:1344-55.

33.   D'Souza A, Sharma S and Boyett MR. CrossTalk opposing view: bradycardia in the trained athlete is attributable to a downregulation of a pacemaker channel in the sinus node. *Journal of Physiology*. 2015;593:1749-51.

34.   Boyett MR, Wang Y, Nakao S, Ariyaratnam J, Hart G, Monfredi O and D'Souza A. Point:Counterpoint debate: Exercise training-induced bradycardia is caused by changes in intrinsic sinus node function. *Journal of Applied Physiology*. 2017;(in press).

35.   Aschar-Sobbi R, Izaddoustdar F, Korogyi AS, Wang Q, Farman GP, Yang F, Yang W, Dorian D, Simpson JA, Tuomi JM, Jones DL, Nanthakumar K, Cox B, Wehrens XH, Dorian P and Backx PH. Increased atrial arrhythmia susceptibility induced by intense endurance exercise in mice requires TNF∝. *Nature Communications*. 2015;6:6018.

36.   Guasch E, Benito B, Qi X, Cifelli C, Naud P, Shi Y, Mighiu A, Tardif JC, Tadevosyan A, Chen Y, Gillis MA, Iwasaki YK, Dobrev D, Mont L, Heximer S and Nattel S. Atrial fibrillation promotion by endurance exercise: demonstration and mechanistic exploration in an animal model. *Journal of the American College of Cardiology*. 2013;62:68-77.

37.   Lv DC, Bei YH, Zhou QL, Sun Q, Xu TZ and Xiao JJ. miR-486 mediates the benefits of exercise in attenuating cardiac fibrosis. *Circulation Research*. 2015;117.

38.   Li X, Wang B, Cui H, Du Y, Song Y, Yang L, Zhang Q, Sun F, Luo D, Xu C, Chu W, Lu Y and Yang B. let-7e replacement yields potent anti-arrhythmic efficacy via targeting beta 1-adrenergic receptor in rat heart. *Journal of Cellular and Moleclar Medicine*. 2014;18:1334-43.

39.   Wang F, Yang XY, Zhao JY, Yu LW, Zhang P, Duan WY, Chong M and Gui YH. miR-10a and miR-10b target the 3'-untranslated region of TBX5 to repress its expression. *Pediatric Cardiology*. 2014;35:1072-9.

40.   Nabialek E, Wanha W, Kula D, Jadczyk T, Krajewska M, Kowalowka A, Dworowy S, Hrycek E, Wludarczyk W, Parma Z, Michalewska-Wludarczyk A, Pawlowski T, Ochala B, Jarzab B, Tendera M and Wojakowski W. Circulating microRNAs (miR-423-5p, miR-208a and miR-1) in acute myocardial infarction and stable coronary heart disease. *Minerva Cardioangiol*. 2013;61:627-637.

41.   Miyamoto S, Usami S, Kuwabara Y, Horie T, Baba O, Hakuno D, Nakashima Y, Nishiga M, Izuhara M, Nakao T, Nishino T, Ide Y, Nakazeki F, Wang J, Ueyama K, Kimura T and Ono K. Expression Patterns of miRNA-423-5p in the Serum and Pericardial Fluid in Patients Undergoing Cardiac Surgery. *Plos One*. 2015;10.

42.   Goldraich LA, Martinelli NC, Matte U, Cohen C, Andrades M, Pimentel M, Biolo A, Clausell N and Rohde LE. Transcoronary gradient of plasma microRNA 423-5p in heart failure: evidence of altered myocardial expression. *Biomarkers*. 2014;19:135-141.

43.   Zicha S, Fernandez-Velasco M, Lonardo G, L'Heureux N and Nattel S. Sinus node dysfunction and hyperpolarization-activated (HCN) channel subunit remodeling in a canine heart failure model. *Cardiovascular Research*. 2005;66:472-481.

44.   Verkerk AO, Wilders R, Coronel R, Ravesloot JH and Verheijck EE. Ionic remodeling of sinoatrial node cells by heart failure. *Circulation*. 2003;108:760-766.

45.   Yanni J, Zi M, Choudhury M, Cai X, Logantha S, Li J, Cartwright E, Dobrzynski H, Hart G and Boyett MR. microRNA 370-3p could explain the dysfunction of the cardiac conduction system in heart failure. *Proceedings of the Physiological Society*. 2015;34:PC158.

46.   Stark A, Brennecke J, Bushati N, Russell RB and Cohen SM. Animal MicroRNAs confer robustness to gene expression and have a significant impact on 3'UTR evolution. *Cell*. 2005;123:1133-46.

FIGURE LEGENDS

Figure 1. **Evidence of a role for HCN4 in the resting bradycardia in human athletes. A**, VO_2max of sedentary human subjects and human athletes (n=7/8). **B**, Heart rates measured under baseline conditions and after complete autonomic blockade of sedentary human subjects and human athletes (n=10/8). **C**, Complete autonomic blockade abolishes heart rate variability. Left, examples traces of RR interval under baseline conditions and after complete autonomic blockade. Right, spectral analyses of corresponding RR interval plots demonstrating near-abolition of high frequency heart rate variability after autonomic blockade (note difference in y-axis scale). PSD, power spectral density. **D**, Relationship between the intrinsic heart rate measured after complete autonomic blockade and VO_2max in sedentary human subjects and human athletes (n= 7/8). **E**, Relationship between ivabradine-induced decrease in heart rate and the intrinsic heart rate measured after complete autonomic blockade in sedentary human subjects and human athletes (n=10/8). In D and E, data fit by linear regression; best fit line, 95% confidence limits, and R^2 and P values shown.

Figure 2. I_f **remodelling in training-induced bradycardia is accompanied by dysregulation of miRs.** **A**, Heart rates of sedentary and trained mice measured in vivo in conscious animals (n=5/9) and in vitro in isolated sinus node preparations (n=6/6). **B**, Expression of HCN4 mRNA in sinus node of sedentary and trained mice (n=5/5). **C**, Current-voltage relationships for I_f recorded from single sinus node cells from sedentary (n=47 cells/5 mice) and trained (n=58 cells/4 mice) mice. **D**, Relationship between ivabradine-induced decrease in heart rate and the intrinsic heart rate measured in vivo after complete autonomic blockade in sedentary and trained mice (n=8/10). Data fit by linear regression; best fit line, 95% confidence limits, and R^2 and P values shown. **E**, Significant (as determined by DeSeq) training-induced changes in miR expression (measured by next generation sequencing) in sinus node of mice. Ratio of miR expression in trained mice to expression in sedentary mice shown on logarithmic scale. Hatched bars indicate significant differences after Benjamini-Hochberg FDR correction (P<0.05). Data obtained from three pooled RNA samples per group (n=2/2). **F**, Verification of training-induced changes in miRs by qPCR. Expression shown in sedentary and trained mice (n=6/7-9). *significant difference between sedentary and trained data (P<0.05).

Figure 3. **HCN4 is a target gene for miR-423-5p. A**, Luciferase reporter assay showing post-transcriptional repression of HCN4 by miRs. H9C2 cells were cotransfected with precursor miR and 3′-UTR of HCN4 cloned into expression vector downstream of luciferase gene. Luciferase activity is shown 24 h after co-transfection with different miRs including a control (scrambled) miR. n=3 batches of cells with 4-5 replicates/batch. **B**, Predicted miR-423-5p binding sites in HCN4 3′-UTR and corresponding sequence of mutant HCN4 3′-UTR tested. **C**, Luciferase reporter assay showing dose-dependent repression of HCN4 by miR-423-5p and loss of repression by mutation of HCN4 3′-UTR. Luciferase activity is shown 24 h after co-transfection with different amounts of wild-type or mutant miR-423-5p. n=3 batches of cells with 4 replicates/batch. **D**, Relationship between HCN4 mRNA and log miR-423-5p in sedentary and trained mice (n=5/5). **E**, Relationship between the heart rate measured in vitro in the isolated sinus node and log miR-423-5p in sedentary and trained mice (n=6/7). In D and E, data fit by linear regression; best fit line, 95% confidence limits, and R^2 and P values shown. **F**, Expression of miR-423-5p (measured by qPCR) in atrium and ventricle is low and unaltered by training. Expression shown in sinus node, right atrial muscle and left ventricular muscle from sedentary and trained mice (n=5/5/5). Inset, data from left ventricular muscle at magnified scale. **G**, Expression of miR-423-5p (measured by qPCR) in sinus node is partially restored on detraining (right). Expression shown in sinus node of sedentary, trained and detrained mice (n=5/9/5). *significantly different from control/sedentary data (P<0.05).

Figure 4: AntimiR to miR-423-5p reverses training-induced bradycardia and blunts HCN4 channel remodelling. A, Time course of exercise training and antimiR administration. **B**, AntimiR abolishes training-induced upregulation of miR-423-5p in sinus node. miR-423-5p (determined by qPCR) in sinus node of vehicle- or antimiR-treated sedentary and trained mice shown (n=6/5/5/5). **C**, AntimiR reverses training-induced bradycardia. Representative ECG traces (recorded from conscious animals) from a vehicle-treated sedentary mouse, vehicle-treated trained mouse and antimiR-treated trained mouse shown on left and mean heart rates (measured in vivo and in isolated sinus node) on right (n=10/12/12 and 9/12/12). **D**, AntimiR reverses training-induced downregulation of HCN4. Western blots using antibodies recognising HCN4 and actin (housekeeper) proteins for sinus node from vehicle-treated sedentary, vehicle-treated trained and antimiR-treated trained mice shown as well as mean expression level of HCN4 protein (normalised to actin) in the three groups (n=5/4/5 with three independent replicates per mouse). **E,** AntimiR reverses training-induced downregulation in contribution of I_f to pacemaking. Percentage decrease in heart rate (recorded from isolated sinus node preparations) on blocking I_f using 2 mM Cs^+ invehicle-treated sedentary, vehicle-treated trained and antimiR-treated trained mice shown (n=6/7/4). **F**, AntimiR reverses training-induced downregulation in I_f. Representative I_f traces (normalised to cell capacitance) from vehicle-treated sedentary, vehicle-treated trained and antimiR-treated trained mice shown on left and mean current-voltage relationships for I_f from vehicle-treated sedentary (n=47 cells/5 animals), vehicle-treated trained (n=58 cells/4 animals) and antimiR-treated trained (n=89 cells/5 animals) mice shown on right. *significantly different (B-E) or significantly different from trained+vehicle data (E; P<0.05).

Figure 5. Nkx2.5 regulation of miR-423-5p. A, map of NSRP1 gene (solid blocks show exons with introns in between) showing location of Nkx2.5 binding sites and intronic location of the miR-423 gene. **B**, Expression of NSRP1 mRNA in sinus node of sedentary and trained mice (n=8/8). **C**, Significant (P<0.05) training-induced changes in expression of transcription factor transcripts (measured by qPCR) in sinus node of mice. Ratio of mRNA expression in trained mice to expression in sedentary mice shown (n=6/8). **D**, Expression of Nkx2.5 mRNA in sinus node of sedentary and trained mice (n=8/8). **E**, Luciferase reporter assay showing activation of NSRP1 transcription by Nkx2.5. H9c2 cells were transfected with 2.1 kb of the 5′ flanking region of NSRP1 cloned into expression vector downstream of gene for luciferase. The cells were co-transfected with Nkx2.5; control cells were not co-transfected with Nkx2.5. Luciferase activity is shown 48 h after transfection. n=3 independent batches of cells with 4 replicates/batch. **F**, Upregulation of miR-423-5p by Nkx2.5. miR-423-5p expression is shown in H9c2 cells not transfected (control) or transfected with Nkx2.5.

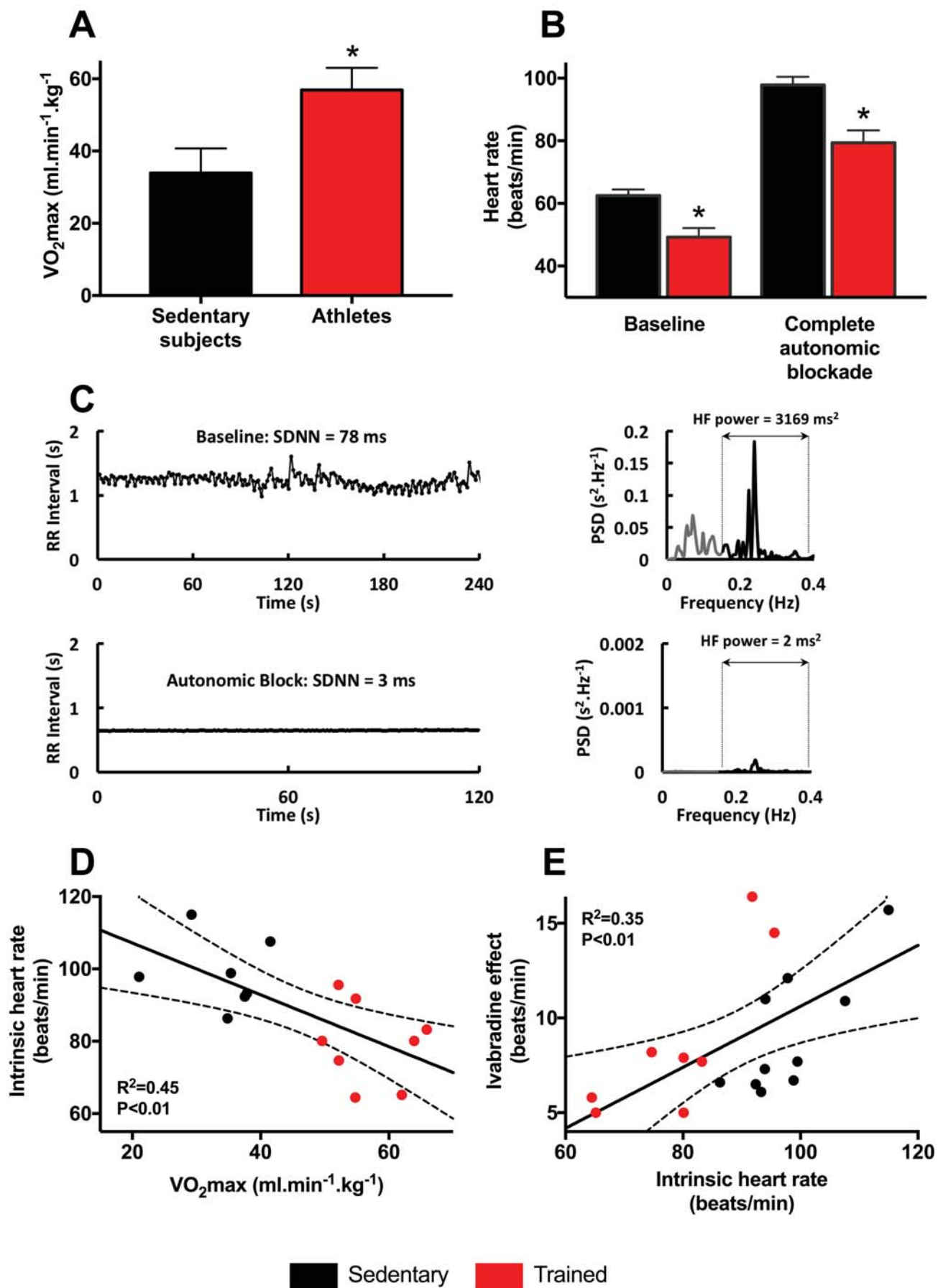**NOVELTY AND SIGNIFICANCE**

What Is Known?

- Athletes have a slow resting heart rate, i.e. sinus bradycardia, and in veteran athletes this can necessitate electronic pacemaker implantation.

- We have previously shown that a downregulation of the key pacemaking ion channel, HCN4, and the corresponding ionic current (funny current or I_f) in the sinus node underlies the sinus bradycardia in rodent models of exercise training.
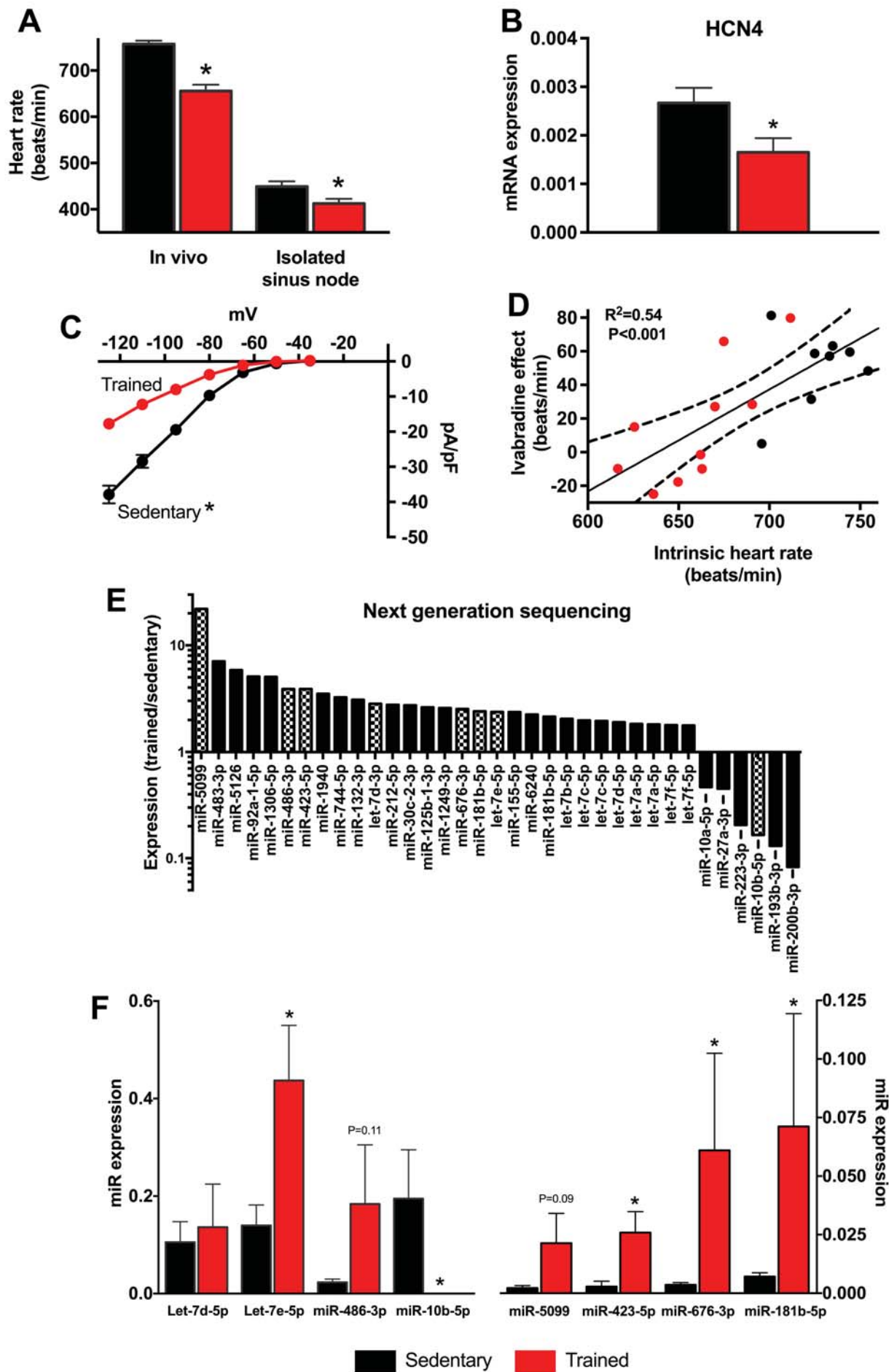
What New Information Does This Article Contribute?

- In human athletes, evidence suggests I_f is also downregulated.

- In the mouse, evidence suggests the downregulation of HCN4 and I_f is the result of an upregulation of Nkx2.5 and, consequently, miR-423-5p.

- In the mouse, the training-induced bradycardia is reversed by blocking the action of miR-423-5p
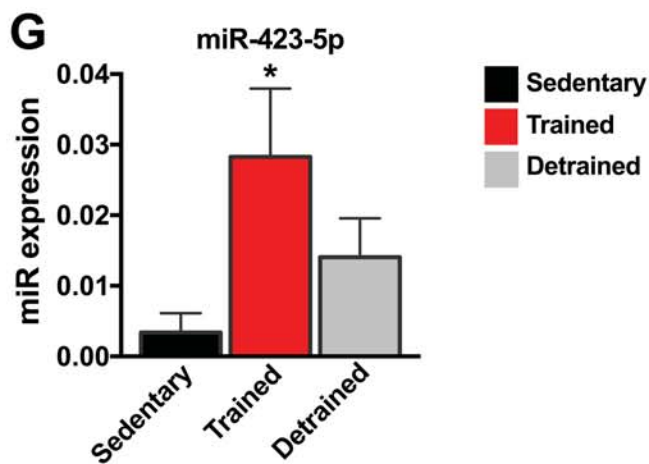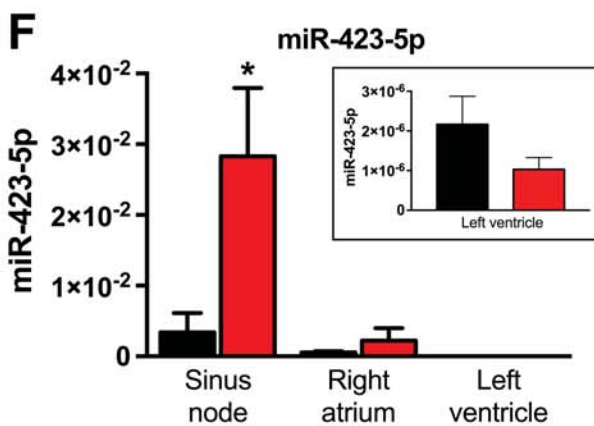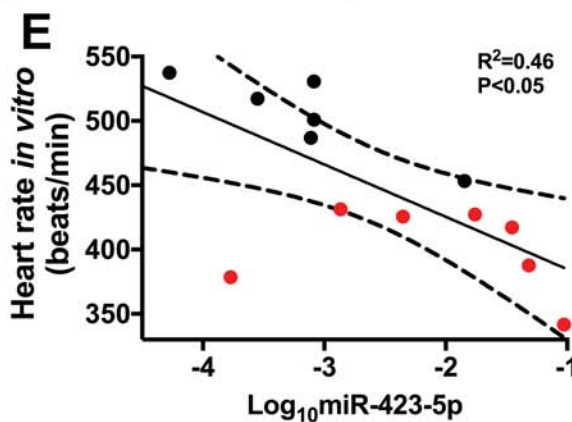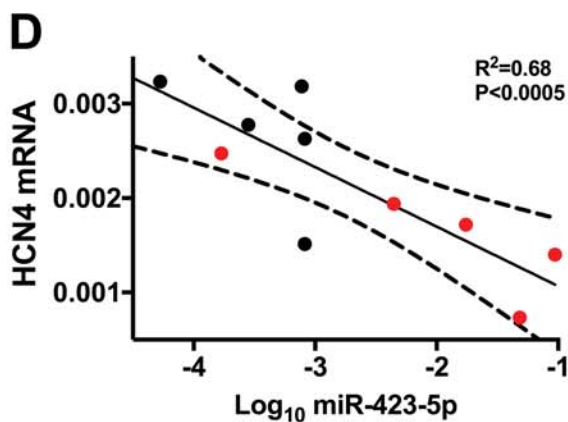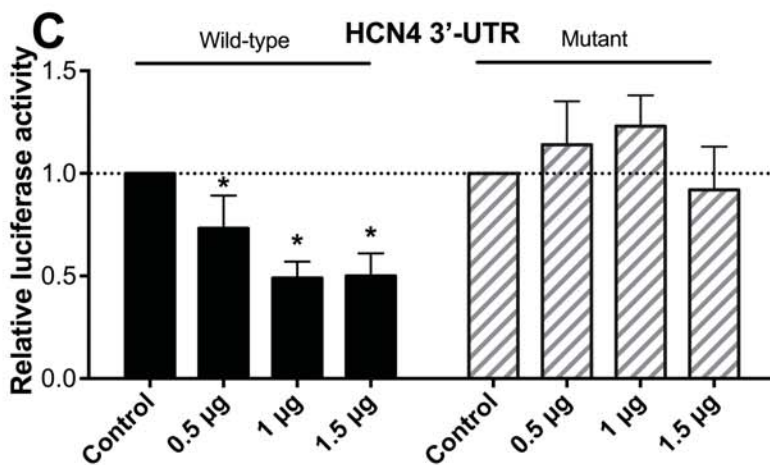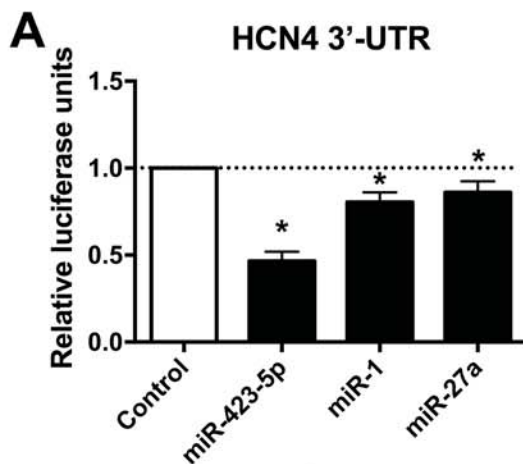
In exercise-trained rodents, we previously attributed the sinus bradycardia to downregulation of I_f. Now we show, in human athletes, the intrinsic heart rate (measured after autonomic blockade) is slower and this is correlated with a smaller response to ivabradine. In the exercise-trained mouse, we then identified an upregulation of miR-423-5p (regulatory microRNA) and Nkx2.5 (transcription factor) – further experiments showed that Nkx2.5 can upregulate miR-423-5p and miR-423-5p can downregulate HCN4. Blocking miR-423-5p with an antimiR reversed the training-induced sinus bradycardia. For the first time, this suggests that there is a downregulation of I_f in human athletes and identifies the pathway involved.

FIGURE 1

Human

FIGURE 2

FIGURE 3

A HCN4 3'-UTR

B

HCN4 3'UTR binding site 1 TGAG-CTGGGCCCTCCCTCCCTCT
                            :|| |||||| |||| :||||||
miR-423-5p   TTTCAGAGC-GAGAGACGGGGAGT

mutant   CGAATGACACGCGTGTCCTTGCGG

HCN4 3'UTR binding site 2 TCTTGCTC-CTTTCT-TCCTTCA
                            |||| ||:||| :||:||
miR-423-5p   TTTCAGAGCGAGAGACGGGGAGT

mutant   GATCGCCGACCGCAGAACTTACG

C HCN4 3'-UTR

D R²=0.68 P<0.0005

E R²=0.46 P<0.05

F miR-423-5p

G miR-423-5p

Sedentary
Trained
Detrained

FIGURE 4

FIGURE 5

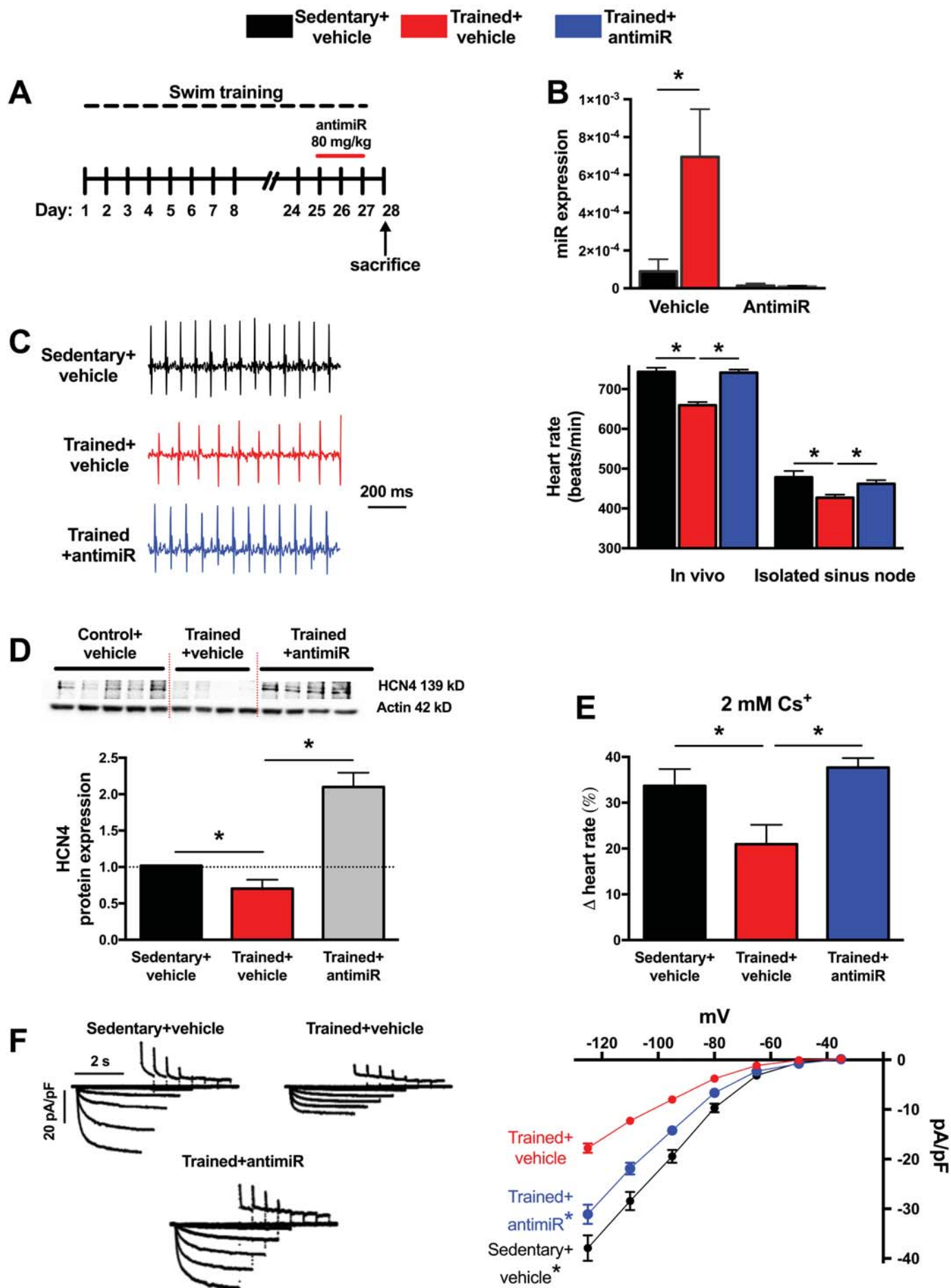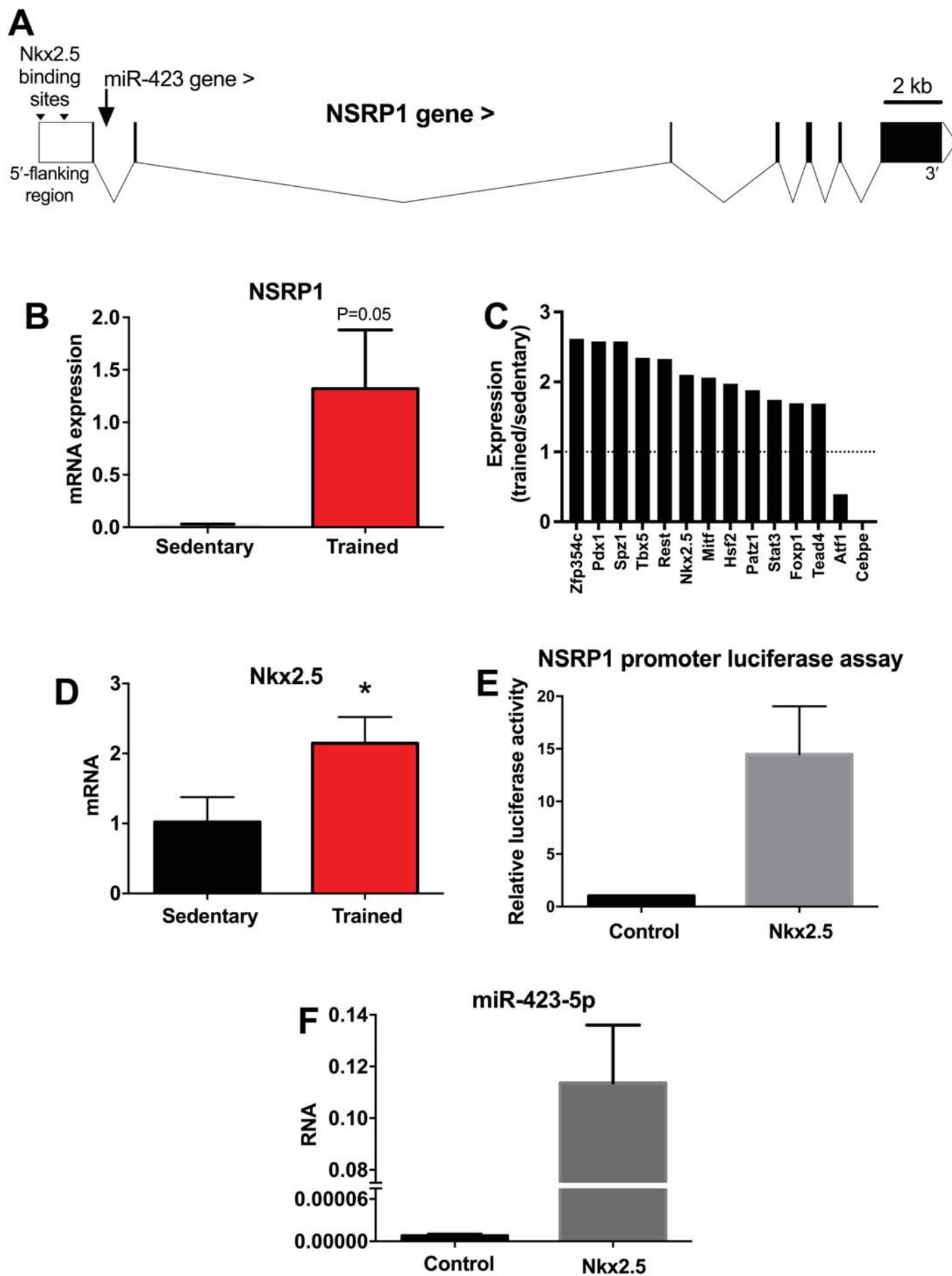# Circulation Research

JOURNAL OF THE AMERICAN HEART ASSOCIATION

Targeting miR-423-5p Reverses Exercise Training-Induced HCN4 Channel Remodeling and Sinus Bradycardia

Alicia D'Souza, Charles M Pearman, Yanwen Wang, Shu Nakao, Sunil Jit R Logantha, Charlotte Cox, Hayley J Bennett, Yu Zhang, Anne Berit Johnsen, Nora Linscheid, Pi C Poulsen, Jonathan Elliott, Jessica Coulson, Jamie S McPhee, Abigail C Robertson, Paula A da Costa Martins, Ashraf Kitmitto, Ulrik Wisloff, Elizabeth J Cartwright, Oliver Monfredi, Alicia Lundby, Halina Dobrzynski, Delvac Oceandy, Gwilym M Morris and Mark R Boyett

The online version of this article, along with updated information and services, is located on the
World Wide Web at:
http://circres.ahajournals.org/content/early/2017/08/17/CIRCRESAHA.117.311607
Free via Open Access

Data Supplement (unedited) at:
http://circres.ahajournals.org/content/suppl/2017/08/17/CIRCRESAHA.117.311607.DC1

Targeting miR-423-5p reverses exercise training-induced HCN4 channel remodelling and sinus bradycardia

Alicia D'Souza, Charles Pearman, Yanwen Wang, Shu Nakao, Sunil Jit R.J. Logantha,
Charlotte Cox, Hayley Bennett, Yu Zhang, Anne Berit Johnsen, Nora Linscheid,
Pi Camilla Poulsen, Jonathan Elliot, Jessica Coulson, Jamie McPhee, Abigail Robertson,
Paula Da Costa Martins, Ashraf Kitmitto, Ulrik Wisloff, Elizabeth J. Cartwright, Oliver Monfredi,
Alicia Lundby, Halina Dobrzynski, Delvac Oceandy, Gwilym M. Morris, Mark R. Boyett

SUPPLEMENTAL METHODS

Human study

Study subjects were male volunteers aged between 18 and 30 years and non-smokers with no known illnesses and taking no medications. The study group were competitive endurance athletes of a good standard, training or competing for a minimum of eight h per week. Control subjects were sedentary age-matched males exercising for less than 2 h per week. Table S1 shows further characteristics of the subjects. The study protocol was approved by the regional research ethics committee and subjects gave informed consent. A three lead ECG was continuously recorded using an AD Instruments Powerlab ECG system. Subjects were studied in a supine position and in the post-absorptive fasted state. Complete autonomic blockade for measurement of the intrinsic heart rate was achieved by intravenous injection of atropine 0.04 mg/kg and propranolol 0.2 mg/kg. Ivabradine 7.5 mg p.o. was given to block the funny current, I_f. At peak plasma ivabradine (1 h), further atropine and propranolol were administered to ensure continued complete autonomic block. The additional dose calculations were based on known pharmacokinetics of atropine and propranolol:

$$C_2 = C_1 e^{-(0.693/t_{1/2})t}$$

where C_2 is the plasma concentration, C_1 is the original plasma concentration, $t^{1/2}$ is the half time of the drugs (4 h) and t is elapsed time since the original injection (1 h). The effect of block of I_f on the intrinsic heart rate was measured at this time. Heart rate was taken as an average over two 5-min periods (baseline) and over a single 5-min period (intrinsic heart rate; intrinsic heart rate+ivabradine). Heart rate variability was assessed in the following manner: continuous single lead ECGs were recorded digitally at 10 kHz using LabChart v7.0. 256 s ECG segments were selected after an appropriate acclimatisation period following each intervention (10 minutes pre-resting ECG, 5 min following intravenous atropine and propranolol, 60 min following oral ivabradine). R wave peaks were identified automatically and RR intervals were exported to Kubios v2.0 for analysis of heart rate variability. RR series were interpolated at 4 Hz. Heart rate variability was assessed in the time and frequency domains with the high frequency band defined as 0.15-0.4 Hz.

Experimental animals

Care and use of laboratory animals conformed to the UK Animals (Scientific Procedures) Act 1986. Ethical approval for all experimental procedures was granted by the University of Manchester. Eight-week-old male C57BL/6J mice (Harlan Laboratories; initial body weight, 20–25 g) were randomly assigned to either sedentary or trained groups. Mice were housed five per cage in a temperature-controlled room (22°C) with a 12 h:12 h light:dark lighting regime and free access to food and water.

Swim training

Mice were subjected to a swimming programme described previously.[1, 2] The mice were swim-trained for 60 min twice daily for 28 consecutive days. All mice were able to complete the course of training. Age- and weight-matched sedentary littermates served as controls for all experimental conditions and were handled daily. Additionally, a cohort of swim-trained mice was submitted to detraining for two weeks after the 28-day training period during which physical activity was restricted to the space of the cage.

Conscious ECG recordings

ECGs were recorded non-invasively in unrestrained, conscious mice using the ECGenie recording enclosure (Mouse Specifics, Inc., Boston, MA, USA) as described previously.[1] Heart rate was measured over 100 consecutive beats. The effect of (6 mg kg^{-1}) ivabradine under complete autonomic block with atropine (0.5 mg kg^{-1}) and propranolol (1 mg kg^{-1}) was measured as previously described.[1]

Unconscious ECG recordings

ECGs were recorded under isofluorane anaesthesia as described previously.[1] 1.5% isoflurane in 100% O_2 with a flow rate of 1 l/min was used. ECG parameters were measured over 100 consecutive beats.

AntimiR design and administration

We employed a previously validated chemistry and administration protocol that has been shown to be highly efficient in knocking down target micro-RNAs (miRs) in the heart with long-lasting efficacy under *in vivo* conditions.[3] Chemically modified antisense nucleotide (antimiR) against miR-423-5p was designed and obtained from Integrated DNA Technology (IDT, Belgium). The sequence of antimiR-423-5p was the exact antisense of the mature miR sequence (obtained from miRbase[4]): 5′-UGAGGGGCAGAGAGCGAGACUUU/3CholTEG with 3′ cholesterol conjugation, two phosphorothioate bonds at the very first 5′ end and four phosphorothioate bonds between the last 3′ bases. These modifications improve cell uptake and protect against nuclease degradation while increasing affinity of the antisense oligonucleotide to the target.[5] Chemically modified antisense oligonucleotides designed to target *C. elegans* miR-39-5p (5′-AAGGCAAGCUGACCCUGAAGUU-3′/3CholTEG-3′) that does not target mammalian sequences[3] was used as a control antimiR. AntimiRs were diluted in sterile saline and administered to mice via intraperitoneal injection on three consecutive days (each day, 80 mg/kg). Vehicle-treated mice were given an equivalent volume of sterile saline.

RNA isolation

Mice were killed by cervical dislocation and a ~1 mm biopsy collected from the sinus node at the level of the main branch from the crista terminalis and a separate biopsy was collected from the neighbouring right atrial free wall. Biopsies were frozen in liquid N_2 and stored at −80°C until use. Total RNA was isolated using an RNeasy Micro kit (Qiagen) according to the manufacturer's instructions. Total RNA was isolated from H9c2 cells using Trizol Reagent in conjunction with Purelink RNA Mini Kit (Life Technologies) according to the manufacturer's instructions. RNA purity and quantity was determined using a NanoDrop ND-1000 spectrophotometer (NanoDrop Technologies, Wilmington, DE, USA).

Quantitative PCR (qPCR) for miRs

miR expression levels were measured using miRCURY LNA (Locked Nucleic Acid) Universal RT microRNA PCR setup (Exiqon, Denmark) using the manufacturer's instructions for cDNA synthesis and qPCR. Primers were purchased from Exiqon (miR-10b-5p, 205637; miR-486-3p, 204107; miR-423-5p, 205624; miR-676-3p, 205098; miR-181b-5p, 204530; Let-7e-5p, 205711; Let-7d-5p, 204124). Primer set for mmu-miR-5099 was custom designed according to previously published sequences. Expression of miR was calculated by the ΔCt method and normalisation to expression of RNU1A1, which was determined as the optimal endogenous control (RNU1A1, SNORD65 and RNU5G were tested) using the algorithm geNorm (qBase[plus], version 2.0, Biogazelle, Belgium).

qPCR for mRNAs

First strand cDNA was synthesised using Superscript II reverse transcriptase (Invitrogen, Carlsbad, CA, USA). qPCR was performed using an ABI Prism 7900 HT Sequence Detection System (Applied Biosystems/Life Technologies Corporation, Carlsbad, CA, USA). The reaction mixture comprised 1 μl of cDNA, 1× Qiagen assay (HCN4, QT00268660; 18S, QT02448075), 1× SYBR Green Master Mix (Applied Biosystems) and DNase-free water. All samples were run in duplicate. The reaction conditions were: denaturation step of 95°C for 10 min followed by 40 cycles of amplification and quantification steps of 95°C for 30 s, 60°C for 30 s and 72°C for 1 min. The melt curve conditions were: 95°C for 15 s, 60°C for 15 s and 95°C for 15 s. mRNA expression was calculated by the ΔCt method and normalisation to the expression of 18S.

qPCR for transcription factors

Expression levels of seven housekeeping genes and 88 selected transcription factors predicted to target 2 kb of the NRSP1 5′ flanking region were measured using custom-designed TaqMan Low density array (TLDA) cards (Life Technologies, cat. no. 4342259; format 96A; transcripts studied are listed in Table S4) according to manufacturer's instructions. 200 ng of total RNA was used as a template in 20 μl reactions to generate cDNA using a High Capacity cDNA Reverse Transcription Kit (Life Technologies). cDNA was then combined with Universal Master Mix (Life Technologies) and applied to each port of a TLDA card organised in eight ports of 48 genes each. Thermal cycling was carried out on an ABI Prism 7900HT according to the manufacturer's recommended

protocol. Amplification plots were analysed using RQ manager (Life Technologies). Ct values were exported to RealTime Statminer (Integromics) data analysis package that enabled advanced filtering of outlier genes, geNorm-based selection of optimal endogenous controls genes Gapdh and Tbp and differential expression testing using the non-parametric Limma test.[6] Transcript expression levels were calculated using the ΔCt method.

Next generation sequencing

Four cDNA libraries (two for sedentary and two for trained groups) were constructed from three pooled samples each. The cDNA libraries were prepared from 1 µg of total RNA using TruSeq Small RNA Sample Prep Kit (Illumina, Inc.) according to the manufacturer's instructions. Briefly, RNA 3′ adapter and RNA 5′ RNA adapter were ligated to each end of small RNA molecules. The ligation products were used as a template for cDNA synthesis using SuperScript II Reverse Transcriptase (Invitrogen) to create single stranded cDNA. The cDNA was then PCR amplified using a common primer and a primer containing index sequences. After RT-PCR amplification, the cDNA libraries were purified by polyacrylamide gel electrophoresis to select libraries containing mature miR and other regulatory small RNAs. 22 and 30 nt bands were extracted from the gel and purified using the MinElute Gel Extraction Kit (Qiagen). The sizes of the selected library were validated by an Agilent Technologies 2100 Bioanalyzer using a High Sensitivity DNA chip.

50 base pair single-end reads were sequenced on the Illumina MiSeq sequencer (Illumina, Inc.) yielding up to 30 million raw reads per sample. Fastq files generated by MiSeq platform were analysed with FastQC (S. Andrews, 2010; *FastQC: a quality control tool for high throughput sequence data*; available online at: http://www.bioinformatics.babraham.ac.uk/projects/fastqc) and any low quality reads and contaminated barcodes and primers trimmed with Trimmomactic.[7] Reads without adaptor sequences and with no ambiguous bases and the final trimmed length of at least 19 nucleotides were included for the final alignment analysis. Libraries were then aligned to mm10 assembly of mouse genome using Tophat 2[8] which incorporates Bowtie, short-read aligner software. Alignments with the best score were reported from each read. The mapped reads were then counted against gff files downloaded from miRbase, mmu.gff3, with HTSeq.[9] Reads were considered as mature miRs if they fulfilled the 'Strict' requirement on HTSeq, i.e. mapped to and within the whole miR range as defined by miRbase. Normalisation (to control for the variation in the number of read sequences across samples) was done using the DESeq Bioconductor package in 'R' based on the geometric mean. After normalised read counts were obtained, differentially expressed miRs were identified by comparing sedentary versus trained samples with DESeq.[10] DESeq is based on the negative binomial distribution and outputs fold change and P values for differential expression. P values were then adjusted for multiple testing using a false discovery rate of 5% via the Benjamini-Hochberg method. miRs with $P<0.05$ were considered to be differentially expressed.

Computational prediction of miR targets and cis-acting transcription factors

We used three established miR target prediction algorithms to investigate whether any differentially expressed miRs identified by next generation sequencing (FDR<0.05) were predicted targets in the regulation of mouse HCN4 based on 3′-UTR binding sites. miRs predicted by two out of three algorithms were considered targets for further analysis by reporter gene assay (miR-423-5p, miR-486-3p). In addition, we also carried out an unbiased search for all candidate miRs that could target HCN4 to find that it was a consistently predicted target for miR-27a-3p and hence this was included in the screen along with miR-1 that has been previously linked to HCN4.[1]

Prediction algorithm	Predicted HCN4-targeting miRs
Targetscan Mouse v7[11]	miR-423-5p, miR-27a-3p, miR-486-3p
PITA[12]	miR-27a-3p, miR-486-3p, miR-1a 3p/5p, Let-7e
RNA22[13]	miR-423-5p, miR-27a-3p, Let-7d

MatInspector (Genomatix, Release 8.4) was used to analyse potential transcription factor binding sites within 2 kb of the 5′ flanking region upstream of the transcription start site of the host gene of

miR-423-5p, NSRP1. On the basis of evolutionary conservation between mice and humans and scores for similarity to canonical binding sites, 79 top predicted transcription factors were selected for further expression profiling along with nine other cardiac transcription factors either known to be involved in function and/or development of the heart (transcripts studied are listed in Table S4).

Plasmids

(i) pmiRGLO-HCN4 3′-UTR. Primer pairs (forward, 5′-GCTAGCCGCTCCAAACTGCCGTCTAAT-3′; reverse, 5′-GTCGACCTCCCTCCCTCCCTCCCTCTC-3′) were used to PCR amplify 192 nt full length mouse HCN4 3′-UTR (NCBI Reference Sequence: NM_001081192.1) from mouse genomic DNA (wild type C57Bl/6). NheI and SalI sites were incorporated in the primers to facilitate cloning. 1 μl of cDNA was PCR amplified using the PfuTurbo Hotstart DNA polymerase (Agilent Technologies) in a 25 μl reaction with 2.5 μl buffer, 0.5 μl dNTPs, 1 μl of each primer (forward/reverse, 100 μM), 0.5 μl polymerase, 20 μl H_20. Cycling conditions (for 30 cycles) were 95°C for 15 min (initial denaturation), 94°C for 15 s (denaturation), 52°C for 30 s (annealing), 72°C for 45 s (extension) and 72°C for 7 min (final extension). Purification of PCR products and plasmid DNA as well as separation of DNA after restriction digests were performed by cutting bands of appropriate size from a 1.5 % agarose gel under UV-light and subsequent purification of DNA from agarose gels with Qiaquick gel extraction kit (Qiagen) according to the manufacturer's instructions. In subsequent cloning steps, 2 μg of pmiRGLO dual luciferase miR target expression vector (Promega, E1330) DNA was digested with 1 μl NheI and 1ul SalI. 8 μl of purified PCR product (amplified HCN4 3′-UTR) was also digested with 1 μl NheI and 1 μl SalI. For subsequent cloning, linearised vector DNA was dephosphorylated following which linearised plasmid DNA and inserts were purified on a 1.5% agarose gel. For ligation, 100 ng of digested vector DNA was incubated with inserts in four different molar ratios (vector to insert 1:3, 1:5, 1:7 or 1:9) along with 1 μl of 10x ligase buffer and 1 μl T4 DNA ligase overnight at 16°C. Competent *E. coli* cells (DH5α, Sigma-Aldrich) were transformed with ligated plasmids. 2 ml LB medium supplemented with ampicillin (final concentration of 100 μg/ml) was inoculated with a single bacterial colony and incubated overnight at 37°C with shaking (250 rpm). Plasmid DNA was purified using the Purelink Plasmid Kit (Thermo Fisher) according to manufacturer's instructions. For analytical restriction digest, plasmid DNA was incubated with the restriction enzymes NheI and SalI for 1.5 h at 37°C to confirm the presence of the correct ligation of 3'UTR inserts in the pmirGLO vector. Mutant HCN4 3'UTR with nucleotide substitutions for two predicted miR-423-5p binding sites was generated by GenScript (USA).

(ii) pcDNA-NKX2.5. pEntr-Nkx2-5flbio containing mouse Nkx2.5 cDNA was a gift from William Pu (Addgene plasmid # 32969). The Nkx2.5 fragment was then transferred to the vector pcDNA6.2 cLumio-DEST (Invitrogen) by using the Gateway vector system (Invitrogen) to produce pcDNA6.2-Nkx2.5 using a protocol recommended by the manufacturer.

(iii) pGL3-NSRP1. A 2.1 kb fragment upstream of the NSRP1 transcription start site, corresponding to the promoter region and encompassing predicted Nkx2.5 binding sites (given in Figure S3) was synthesised by Dundee Cell Products. The fragment was then directionally subcloned into a luciferase containing plasmid, pGL3-basic (Promega) reporter using Kpn I and Hind III cloning sites, which were incorporated to the NSRP1 promoter construct, to generate a NRSP1 promoter luciferase construct.

Cell culture, transfection and reporter assays

H9c2 cells were maintained in Dulbecco's modified Eagle's medium (DMEM) (Invitrogen) supplemented with 10% foetal bovine serum and 1% penicillin/streptomycin. For Nkx2.5 overexpression, 5 x10^5 cells /well were plated in 6-well plates 24 h prior to transfection with 3 μg pcDNA3.1-Nkx2.5 or pcDNA3.1 empty vector. For reporter assays investigating miRs, cells were seeded at a density of 10^5cells/well in 24-well plates 24 h prior to transfection and co-transfected with 500 ng HCN4 3′-UTR plasmid or mutant and 0.5-1.5 μg precursor miR or negative control plasmid. For reporter assays testing NRSP1 promoter activity, the same procedures were followed to co-transfect H9C2 cells with 1 μg of promoter-luciferase fusion plasmid pGL3 and pcDNA-Nkx2.5 or negative control. Lipofectamine 2000 (Invitrogen) was used for all transfections according to the manufacturer's instructions. Transfected cells were incubated with DNA-Lipofectamine complexes for 24 h before lysing in passive lysis buffer (Promega) for luciferase assay or washed with phosphate buffered saline (PBS) and incubated for a further 24 h with 2 ml of fresh DMEM before lysis in Trizol (Invitrogen) for RNA extraction. Luciferase activity was determined using a Luciferase Assay System (Promega) using 10 μl of cell lysate on a

luminometer (Berthold Technologies Lumat LB 9507). For each luminescence reading the injector was programmed to dispense 50 µl assay reagent after which there was a 2 s pre-measurement delay followed by a 7 s measurement period. Luciferase assays were performed in quadruplicate and repeated three times with an independent batch of cells. For miRs Firely luciferase and renilla luciferase activity were measured and data were analysed based on ratio of Firely/Renilla activity.

Western blot

HCN4 protein levels were determined by western blot using previously described methods.[14] Briefly, protein lysate was obtained by homogenising snap frozen sinus node biopsies using an MP FastPrep-24 5[G] and 2 ml tubes containing FastPrep metal bead lysing matrix (1.4 mm) in RIPA buffer (Sigma Aldich)**.** Total protein concentration was estimated using Bradford protein assay against standard curve of bovine serum albumin (BSA; 0-0.5 mg/ml) following which samples were denatured by adding final volume of 25% SDS-sample buffer - 100 mM Tris-HCl, pH 6.8, 25% (v/v) glycerol, 10% (v/v) SDS, 10% (v/v) β-mercaptoethanol, 0.1% (w/v) bromophenol blue - and heating to 80°C for 10 min. Samples were loaded onto a 12% stain-free SDS-polyacrylamide gel (Bio-Rad) with PreSciccion Plus (Bio-Rad) protein standards and run at 50 mV for ~50 min in SDS running buffer (25 mM Tris, 192 mM glycine, 0.1% SDS). Stain-free gels were imaged using ChemiDoc MP and then transferred to PVDF (polyvinyl difluoride) membranes using a Trans-Blot Turbo transfer system (Bio-Rad) at 15 V/0.3 mA for 15 min. PVDF membranes (activated in 100% ethanol before use) and thick filter paper were pre-wet in transfer buffer - 1x Trans-Blot Turbo transfer buffer (Bio-Rad) and 20% (v/v) ethanol. Successful transfer was confirmed by using the ChemiDoc MP. PVDF membranes were washed in TBS for 5 min and then blocked in milk-TBS-Tween (5% w/v non-fat dried Marvel milk, 0.1% v/v TBS and Tween 20) for 1 h at room temperature with gentle rocking. The membranes were then probed with the following primary antibodies for 1 h at room temperature with gentle rocking: rabbit polyclonal anti-HCN4 (Alomone labs), 1:100; rabbit polyclonal anti-actin (Sigma Aldrich), 1:1000. Following three 10 min washes in TBS-Tween, membranes were then probed with horseradish peroxidase (HRP)-linked secondary antibody (HRP-linked anti-rabbit IgG, Cell Signalling) for a further 1 h at room temperature with gentle rocking. Membranes were then washed three times for 5 min in TBS-Tween to remove unbound secondary antibody. Chemiluminescence was achieved by the addition of Clarity Western ECL substrate (Bio-Rad) in a 1:1 ratio for 5 min in the dark. Membranes were then imaged with the ChemiDoc MP. Sedentary, trained and trained+antimiR samples were run on the same gel to ensure identical exposure conditions. The chemiluminescent signal intensity was normalised to the relative quantification of the corresponding intensity of actin. Data from each replicate were normalised and averaged across replicates.

Proteomics

Mass spectrometry based proteomics experiments were performed to evaluate protein expression of selected targets in isolated sinus node biopsies from sedentary male C57BL/6J mice (n=30 pooled into 3 samples with 10 biopsies in each sample). Briefly, sinus node biopsies were collected and immediately snap frozen in liquid N_2 and stored at -80°C until processing. Cardiac proteins were extracted from the biopsies and 1 mg protein from each sample was digested as described previously.[15, 16] Peptides were desalted and fractionated by micro-flow reverse-phase ultra high pressure liquid chromatography into 12 fractions. Fractionated peptide samples were analyzed by online reversed-phase liquid chromatography coupled to a Q-Exactive Plus quadrupole Orbitrap tandem mass spectrometer. Peptide samples were separated on 15 cm fused-silica emitter columns using a 1 h multi-step linear gradient. Raw mass spectrometry data was processed using MaxQuant software (version 1.5.3.30) and proteins were identified with the built-in Andromeda search engine using a database containing all reviewed mouse SwissProt protein entries. Analysis of protein abundance was based on summed mass spectrometry-based protein intensities as determined by MaxQuant.

TUNEL assay

The right atrial wall including the sinus node of sedentary and trained mice were quickly dissected, flash frozen with liquid N_2, and stored at -80°C until processing. The tissues were cryosectioned at 12 µm thick and mounted every five sections on an adhesion glass slide. Terminal deoxynucleotidyl transferase biotin-dUTP nick-end labelling (TUNEL; Roche, 11 684 795 910) was then performed combined with standard immunohistochemistry to label the sinus node using anti-HCN4 antibody. Briefly, frozen sections were fixed in 10% neutral buffered formalin, permeabilised in 0.1% triton X-100 in PBS, and blocked with 1% BSA, followed by incubation in rabbit polyclonal

anti-HCN4 antibody (Alomone, APC-052, 1:200 dilution) at 4°C overnight. TUNEL was then carried out at 37°C for 60 min, according to the manufacturer's instruction. Cy3-conjugated anti-donkey and rabbit IgG secondary antibody (Merck Millopore, AP182C, 1:200 dilution) was added in the TUNEL reaction mix. As a positive control, sinus node sections were treated with micrococcal nuclease (ThermoFisher Scientific, EN0181, 30 U/ml). Images of HCN4-positive areas indicating the sinus node region were acquired using a laser scanning microscope (Zeiss LSM 5 PASCAL) equipped with a x40/1.0 PL Apo objective. The confocal settings were as follows: confocal aperture, 200 µm; scan speed, 1.60 µs pixel time, unidirectional; image size, 512 x 512 pixels. Images were acquired using the following conditions: 488 nm excitation and 505-530 nm emission for TUNEL, and 543 nm excitation and >560 nm emission for Cy3, respectively. To count the number of TUNEL-positive cells, images of HCN4-positive regions were combined and the contrast was enhanced using Adobe Photoshop. TUNEL positive cells per section were counted using Cell Counter of ImageJ at five different levels of the sinus node in five sedentary and trained mice.

Tissue electrophysiology

The beating rate of the isolated sinus node was determined by extracellular potential recording as described by Yamamoto *et al.*[17] In brief, animals were weighed and then killed by cervical dislocation following which a right atrial preparation encompassing the sinus node was rapidly dissected in Tyrode solution containing (in mM): 100 NaCl, 4 KCl, 1.2 $MgSO_4$, 1.2 KH_2PO_4, 1.8 $CaCl_2$, 25 $NaHCO_3$ and 10 glucose bubbled with 95% O_2 and 5% CO_2 to give a pH of 7.4. The preparation was superfused with 37°C Tyrode solution at a flow rate of 10 ml/min and extracellular potentials recorded using bipolar electrodes 100 µm in diameter. Recording electrodes interfaced with a Neurolog system (Digitimer) with low-pass and high-pass filters adjusted to optimise the signal-to-noise ratio. Extracellular potentials were continuously recorded for 20 min using a PC with a PowerLab and LabChart v7 software (ADInstruments) following which the effect of 2 mM CsCl (Sigma-Aldrich) on the beating rate was studied. The superfusing solution was changed to Tyrode solution containing 2 mM CsCl. After 15 min of treatment, the rate was recorded for 5 min. The preparation was then washed of CsCl for 20 min, during which the beating rate approached baseline values. The calculated rate was averaged over 500 beats.

Intracellular action potential recording

Intracellular action potentials were recorded in right atrial preparations containing the intact sinus node. Tissue was pinned to a specially designed chamber that allowed epicardial and endocardial contact with superfusing Tyrode solution (containing in mM: NaCl 120.3, KCl 4.0, $CaCl_2$ 1.2, $MgSO_4$ 1.3, NaH_2PO_4 1.2, $NaHCO_3$ 25.2 and glucose 11) bubbled with 95% O2 and 5% CO2 to give a pH of 7.4. Tyrode solution was circulated at 20 ml/min and tissues maintained at 37°C. The leading pacemaker site in the sinus node was mapped with bipolar extracellular electrodes as described in the preceding section. Using 3 M KCl filled sharp microelectrodes of 20-40 MΩ electrical resistance, intracellular action potentials were recorded at the leading pacemaker site of the sinus node and pectinate muscle (atrial tissue). Data acquired at 20 kHz was passed through a 10 kHz low‐pass Bessel filter and amplified 10x by Axon Instruments GeneClamp 500 amplifier (Molecular Devices Inc), digitized with Axon Instruments Digidata 1440A (Molecular Devices Inc), and recorded onto a computer using the WinEDR v3.3.6 program (Dr. J. Dempster, University of Strathclyde, Glasgow, UK). Series of five consecutive action potentials were exported to LabChart v8 software (ADInstruments) and the following action potential parameters were measured: cycle length (interval between consecutive action potential peaks, ms), maximum diastolic potential (MDP, mV), maximum upstroke velocity (dV/dt_{max}, mV/s), action potential height/amplitude (mV), action potential width (interval between consecutive maximum diastolic potentials, ms) and action potential duration (APD, ms) at 10, 50, 70 and 90% repolarization. Heart rate (beats per minute, bpm) was calculated from cycle length measurements for individual observations. GraphPad Prism 6 (GraphPad Software, Inc.) was used for statistical analysis.

Sinus node cell isolation and patch-clamp electrophysiology

Mice were killed by cervical dislocation. After quick removal of the heart, the sinus node tissue was dissected out and strips of nodal tissue were dissociated into single cells by a standard enzymatic and mechanical procedure.[18] The enzyme solution contained collagenase IV (224 U ml^{-1}, Worthington), elastase (1.42 U ml^{-1}, Sigma-Aldrich) and protease (0.45 U ml^{-1}, Sigma-Aldrich).[18] Isolated sinus node cells were stored at 4°C for the day of the experiment. I_f was recorded using a patch electrode in whole-cell mode during superfusion of a Tyrode solution containing (in mM): 140 NaCl, 5.4 KCl, 1.8 $CaCl_2$, 1 $MgCl_2$, 5 HEPES-NaOH, 10 D-glucose, pH 7.4. $BaCl_2$ (1 mM) and

MnCl$_2$ (2 mM) were added to avoid contamination from other ionic currents. The bath temperature was 35±0.5°C. The pipette solution contained (in mM): 130 K-aspartate, 10 NaCl, 2 CaCl$_2$ (pCa=7), 2 MgCl$_2$, 10 HEPES, 5 EGTA, 2 ATP(Na$_2$), 0.1 GTP, 5 creatine phosphate, pH 7.2. To obtain current densities, currents were measured during steps to the range −35 to −125 mV from a holding potential of −35 mV and normalised to cell capacitance. Data were acquired at 1 kHz using an Axopatch 200 amplifier and pClamp 8 (Molecular Devices, Sunnyvale, CA, USA). Data were analysed off-line using Clampfit 10 (Molecular Devices), Origin 8 (Origin Lab Corp., Northampton, MA, USA) and GraphPad Prism 6 (GraphPad Software, Inc.).

Statistical analysis

Statistical analysis was carried out using GraphPad Prism 6 or 7 (GraphPad Software, Inc.) or SPSS (IBM). Two groups were analysed using an unpaired Student's *t*-test (two tailed). When the null hypothesis of equal variance was rejected, an unpaired t-test with Welch's correction was used. If the data were not normally distributed, a non-parametric test (Mann-Whitney test) was used instead of the unpaired t-test. To compare multiple groups, an ANOVA (one- or two-way) was used in the case of normally distributed data and the Kruskal-Wallis test in the case of data not normally distributed. $P<0.05$ was regarded as significant. $0.12>P<0.05$ was regarded of potential interest and the precise P value is given. In figures, data are shown as means±SEM; asterisks indicate significance. For TLDA cards, a non-parametic Limma test was used to compare differences between sedentary and control animals.[6] Statistical analysis of the next generation sequencing data is described above.

SUPPLEMENTAL DISCUSSION

Intrinsic heart rate of untrained, young, male, human subjects

Jose and Collinson[19] reported the intrinsic heart rate for 139 male subjects (non-athletes) between the ages of 20 and 30. This is the first and largest study of the intrinsic heart rate. We have data for 10 male subjects (non-athletes) between the ages of 20 and 30. Although the intrinsic heart rate in this study (97.9±2.6 beats/min) is statistically different (Student's t test; P=0.002) from the intrinsic heart rate (105.6±0.6 beats/min) reported by Jose and Collinson,[19] it is within the mean ± 2× standard deviations from the study of Jose and Collinson.[19] The mean ± 2× standard deviations encompasses 95.4% of the data from the Jose and Collinson[19] study. Previously, we have put this forwards as a criterion for acceptance of intrinsic heart rate data.[20] Whereas the intrinsic heart rate of untrained, young, male, human subjects falls within this acceptable range in some studies, lower values (the lowest being 83.1 beats/min) have been reported in other studies;[20] in all these studies the number of human subjects was 10 or less and, in this respect, have to be considered less definitive than the study of Jose and Collinson.[19] The intrinsic heart rate of young, male subjects (non-athletes) should be approximately the same in different studies. The low intrinsic heart rates reported in some studies are likely to be the result of a technical issue, because the only factors known to decrease the intrinsic heart rate (age,[19] heart failure[21] and athletic training[e.g.22]) are unlikely to apply.

Reported evidence of exercise training-induced increase of vagal tone

Based on block of autonomic tone using atropine and propranolol, we have found no evidence of altered autonomic tone and in particular high vagal tone in human athletes (this study; Figure 1B) and exercise trained C57BL/6J mice.[1] However, again based on block of autonomic tone using atropine and propranolol, Guasch *et al.*[23] (using the Wistar rat) and Aschar-Sobbi *et al.*[24] (using the CD1 mouse) have recently reported evidence of high vagal tone following exercise training (although, strangely, Guasch *et al.*[23] stated that there was no exercise training-induced bradycardia in their study). The cause of the discrepancy is unknown, although it could be the result of an unknown technical issue, the doses of atropine and propranolol used, species used, strain of mouse used, and differences in the duration, intensity and type of training.

We have reviewed the role of high vagal tone (assessed by pharmacological block of autonomic tone) in exercise training-induced bradycardia in the human and animal models.[20] In all studies of human athletes in which the measurement of the intrinsic heart rate is deemed to be correct (see above) there is no evidence of high vagal tone.[20] In nine animal studies, the data suggests that high vagal tone accounts for 76% (mouse), 40% (rat), 43.6% (rat), 10% (rat), 0% (rat), 0% (rat), 0% (rat), 0% (rat) and 0% (rat) of the exercise training-induced bradycardia.[20] Aschar-Sobbi *et al.*[24] state that high vagal tone accounts for 100% of the exercise training-induced bradycardia in the mouse. This is a higher contribution than any of the previous studies. In

contrast, in the mouse we have argued that its contribution is 0%,[1] consistent with five of the previous studies. Also in our case, we have based our conclusion not only on autonomic blockade *in vivo* in the mouse; we have also based it on intrinsic heart rate measurements from the isolated sinus node from both the rat and mouse.[1] Furthermore, we have shown that there is an exercise training-induced downregulation of HCN4 mRNA, HCN4 protein and funny current in the rat and mouse and the exercise training-induced bradycardia is abolished on block of funny current in the mouse (this study and D'Souza *et al.*[1]).

We conclude that it is likely that downregulation of funny current is playing a role in exercise training-induced bradycardia. However, the evidence from Guasch *et al.*[23] and Aschar-Sobbi *et al.*[24] of exercise training-induced high vagal tone is difficult to refute and perhaps high vagal tone could play a role in some circumstances.

Nkx2.5 expression in the adult sinus node

While much is known about the regulatory networks at play in the embryonic development of the cardiac conduction system, the transcriptional networks maintaining function of the adult sinus node are comparatively understudied. The data presented in Online Table IV, as far as we are aware, is the first large scale transcriptomic analysis of transcription factors within the adult mouse sinus node. In Online Figure XA, data from Online Table IV are plotted to show expression levels of 88 transcription factors in the sedentary adult mouse sinus node. Transcriptionally, Nkx2.5 (red bar) is the ninth most abundant transcription factor (of the transcription factors measured). Expression levels of well-known transcription factors in the sinus node (Tbx3, Tbx18 and Shox2) are highlighted in blue for comparison. Online Figure XB shows the protein expression level of selected transcription factors (measured by mass spectrometry) in the sedentary adult mouse sinus node. This confirms the presence of Nkx2.5 in the adult mouse sinus node. Finally, in recent work, Wu *et al.*[25] found that H3K4me3 modifications (a prominent active histone mark associated with active genes) were highly enriched in the Nkx2.5 promoter in the mouse sinus node. In summary, these observations suggest that there is baseline expression of Nkx2.5 in the sinus node (which is then increased in response to exercise training).

<div align="center">

REFERENCES

</div>

1.   D'Souza A, Bucchi A, Johnsen AB, Logantha SJ, Monfredi O, Yanni J, Prehar S, Hart G, Cartwright E, Wisloff U, Dobryznski H, DiFrancesco D, Morris GM and Boyett MR. Exercise training reduces resting heart rate via downregulation of the funny channel HCN4. *Nature Communications*. 2014;5:3775.

2.   Liu W, Zi M, Jin J, Prehar S, Oceandy D, Kimura TE, Lei M, Neyses L, Weston AH, Cartwright EJ and Wang X. Cardiac-specific deletion of *Mkk4* reveals its role in pathological hypertrophic remodeling but not in physiological cardiac growth. *Circulation Research*. 2009;104:905-14.

3.   Dirkx E, Gladka MM, Philippen LE, Armand AS, Kinet V, Leptidis S, El Azzouzi H, Salic K, Bourajjaj M, da Silva GJ, Olieslagers S, van der Nagel R, de Weger R, Bitsch N, Kisters N, Seyen S, Morikawa Y, Chanoine C, Heymans S, Volders PG, Thum T, Dimmeler S, Cserjesi P, Eschenhagen T, da Costa Martins PA and De Windt LJ. Nfat and miR-25 cooperate to reactivate the transcription factor Hand2 in heart failure. *Nature Cell Biology*. 2013;15:1282-93.

4.   Kozomara A and Griffiths-Jones S. miRBase: annotating high confidence microRNAs using deep sequencing data. *Nucleic Acids Res*. 2014;42:D68-73.

5.   Bang C, Batkai S, Dangwal S, Gupta SK, Foinquinos A, Holzmann A, Just A, Remke J, Zimmer K, Zeug A, Ponimaskin E, Schmiedl A, Yin X, Mayr M, Halder R, Fischer A, Engelhardt S, Wei Y, Schober A, Fiedler J and Thum T. Cardiac fibroblast-derived microRNA passenger strand-enriched exosomes mediate cardiomyocyte hypertrophy. *Journal of Clinical Investigation*. 2014;124:2136-46.

6.   Jeanmougin M, de Reynies A, Marisa L, Paccard C, Nuel G and Guedj M. Should we abandon the t-test in the analysis of gene expression microarray data: a comparison of variance modeling strategies. *PloS one*. 2010;5:e12336.

7.   Bolger AM, Lohse M and Usadel B. Trimmomatic: a flexible trimmer for Illumina sequence data. *Bioinformatics*. 2014;30:2114-20.

8.   Kim D, Pertea G, Trapnell C, Pimentel H, Kelley R and Salzberg SL. TopHat2: accurate alignment of transcriptomes in the presence of insertions, deletions and gene fusions. *Genome Biology*. 2013;14:R36.

9.   Anders S, Pyl PT and Huber W. HTSeq - a Python framework to work with high-throughput sequencing data. *Bioinformatics*. 2015;31:166-9.

10.   Anders S and Huber W. Differential expression analysis for sequence count data. *Genome Biology*. 2010;11:R106.

11.   Miranda KC, Huynh T, Tay Y, Ang YS, Tam WL, Thomson AM, Lim B and Rigoutsos I. A pattern-based method for the identification of microRNA binding sites and their corresponding heteroduplexes. *Cell*. 2006;126:1203-17.

12.   Kertesz M, Iovino N, Unnerstall U, Gaul U and Segal E. The role of site accessibility in microRNA target recognition. *Nat Genet*. 2007;39:1278-84.

13.   Agarwal V, Bell GW, Nam JW and Bartel DP. Predicting effective microRNA target sites in mammalian mRNAs. *eLife*. 2015;4.

14.   Pinali C, Bennett HJ, Davenport JB, Caldwell JL, Starborg T, Trafford AW and Kitmitto A. Three-dimensional structure of the intercalated disc reveals plicate domain and gap junction remodeling in heart failure. *Biophysics Journal*. 2015;108:498-507.

15.   Lundby A, Rossin EJ, Steffensen AB, Acha MR, Newton-Cheh C, Pfeufer A, Lynch SN, Consortium QTIIG, Olesen SP, Brunak S, Ellinor PT, Jukema JW, Trompet S, Ford I, Macfarlane PW, Krijthe BP, Hofman A, Uitterlinden AG, Stricker BH, Nathoe HM, Spiering W, Daly MJ, Asselbergs FW, van der Harst P, Milan DJ, de Bakker PI, Lage K and Olsen JV. Annotation of loci from genome-wide association studies using tissue-specific quantitative interaction proteomics. *Nature Methods*. 2014;11:868-74.

16.   Lundby A, Andersen MN, Steffensen AB, Horn H, Kelstrup CD, Francavilla C, Jensen LJ, Schmitt N, Thomsen MB and Olsen JV. In vivo phosphoproteomics analysis reveals the cardiac targets of beta-adrenergic receptor signaling. *Science Signaling*. 2013;6:rs11.

17.   Yamamoto M, Honjo H, Niwa R and Kodama I. Low frequency extracellular potentials recorded from the sinoatrial node. *Cardiovascular Research*. 1998;39:360-372.

18.   DiFrancesco D, Ferroni A, Mazzanti M and Tromba C. Properties of the hyperpolarizing-activated current (i_f) in cells isolated from the rabbit sino-atrial node. *Journal of Physiology*. 1986;377:61-88.

19.   Jose AD and Collison D. The normal range and determinants of the intrinsic heart rate in man. *Cardiovascular Research*. 1970;4:160-167.

20.   Boyett MR, D'Souza A, Zhang H, Morris GM, Dobrzynski H and Monfredi O. Viewpoint: Is the resting bradycardia in athletes the result of remodelling of the sinoatrial node rather than high vagal tone? *Journal of Applied Physiology*. 2013;114:1351-1355.

21.   Jose AD and Taylor RR. Autonomic blockade by propranolol and atropine to study intrinsic myocardial function in man. *Journal of Clinical Investigation*. 1969;48:2019-2031.

22.   Katona PG, McLean M, Dighton DH and Guz A. Sympathetic and parasympathetic cardiac control in athletes and nonathletes at rest. *Journal of Applied Physiology*. 1982;52:1652-1657.

23.   Guasch E, Benito B, Qi X, Cifelli C, Naud P, Shi Y, Mighiu A, Tardif JC, Tadevosyan A, Chen Y, Gillis MA, Iwasaki YK, Dobrev D, Mont L, Heximer S and Nattel S. Atrial fibrillation promotion by endurance exercise: demonstration and mechanistic exploration in an animal model. *Journal of the American College of Cardiology*. 2013;62:68-77.

24.   Aschar-Sobbi R, Izaddoustdar F, Korogyi AS, Wang Q, Farman GP, Yang F, Yang W, Dorian D, Simpson JA, Tuomi JM, Jones DL, Nanthakumar K, Cox B, Wehrens XH, Dorian P and Backx PH. Increased atrial arrhythmia susceptibility induced by intense endurance exercise in mice requires TNF∝. *Nature Communications*. 2015;6:6018.

25.   Wu M, Peng S, Yang J, Tu Z, Cai X, Cai CL, Wang Z and Zhao Y. Baf250a orchestrates an epigenetic pathway to repress the Nkx2.5-directed contractile cardiomyocyte program in the sinoatrial node. *Cell Research*. 2014;24:1201-13.

AUTHOR CONTRIBUTIONS

Online Table I. Characteristics of human subjects. All athletes participated in endurance sports (running, n=4; triathalon, n=3; cycling n=1). BMI, body mass index; SDNN, standard deviation of normal to normal beats; cSDNN, heart rate corrected SDNN.

	Control subjects (n = 10)	Athletes (n = 8)	P value
Gender	male	male	
Age (years)	21.0 ± 0.7	25.9 ± 1.2	**0.002**
Weight (kg)	69.5 ± 1.9	69.8 ± 3.8	0.95
BMI ($kg.m^{-2}$)	21.5 ± 0.7	22.0 ± 078	0.61
Systolic blood pressure (mmHg)	126.6 ± 3.8	120.9 ± 5.7	0.40
Diastolic blood pressure (mmHg)	70.9 ± 3.4	65.4 ± 4	0.30
Heart rate(beats/min)	62.5 ± 1.9	49.2 ± 2.9	**0.002**
SDNN (ms)	64.7 ± 7.3	72.1 ± 9.1	0.43
cSDNN (ms)	185.6 ± 18.6	173.6 ± 23.7	0.69

Online Table II. Intracellular action potential parameters from control mice (sinus node from 4 mice and right atrium from 3 mice) and exercise trained mice (sinus node from 8 mice and right atrium from 5 mice). APD_{10} etc., action potential duration at 10% repolarization etc. Significant differences highlighted by P values in bold font.

	Control	Trained	P value
Sinus node (control, n=65 impalements; trained, n=43)			
Cycle length (ms)	0.12±0.0006	0.12±0.0011	**0.0001**
Spontaneous rate (beats/min)	521±2.9	498±4.9	**0.0001**
Maximum diastolic potential (mV)	-53.3±1.1	-50.0±1.2	**0.046**
Height (mV)	44.8±1.7	39.40±1.1	**0.0087**
APD_{10} (ms)	9.1±0.4	9.4±0.2	0.45
APD_{50} (ms)	28.3±0.5	28.6±0.4	0.67
APD_{70} (ms)	38.1±0.6	39.3±0.6	0.18
APD_{90} (ms)	66.0±1.2	70.2±1.3	**0.021**
Action potential width (ms)	95.4±0.9	100.9±1.4	**0.0007**
Right atrium (control, n=12 impalements; trained, n=26 impalements)			
Maximum diastolic potential (mV)	-80.9±1.2	-79.5±0.8	0.32
Height (mV)	96.7±1.6	94.3±1.5	0.32
APD_{10} (ms)	1.8±0.1	1.7±0.1	0.83
APD_{50} (ms)	11.7±0.4	10.7±0.5	0.17
APD_{70} (ms)	19.7±0.5	17.3±0.8	**0.017**
APD_{90} (ms)	35.3±0.5	31.2±1.2	**0.0029**
Action potential width (ms)	96.8±3.9	98.5±3.6	0.77

Online Table III. Differentially expressed miRs in sedentary and trained mice determined by next generation sequencing. Significant FDR-corrected P values in bold font.

Mature miR	Sedentary mice (DESeq normalised read count)	Trained mice (DESeq normalised read count)	Fold change (trained/ sedentary)	P value	FDR corrected P value
mmu-miR-5099	22.21487273	489.4265862	22.03148279	0.00000	**0.00000**
mmu-miR-423-5p	313.9750531	1219.565294	3.884274506	0.00000	**0.00001**
mmu-miR-486-3p	156.2892445	607.1240921	3.88461851	0.00000	**0.00003**
mmu-let-7d-3p	1235.448761	3484.464362	2.820403786	0.00001	**0.00187**
mmu-let-7e-5p	755.0028997	1800.342372	2.384550274	0.00031	**0.03533**
mmu-miR-181b-5p	278.6639706	674.6823965	2.421132503	0.00035	**0.03533**
mmu-miR-10b-5p	421.1952422	69.86093779	0.165863549	0.00035	**0.03533**
mmu-miR-676-3p	350.2394139	879.8612085	2.512170743	0.00040	**0.03533**
mmu-miR-92a-1-5p	7.942430494	40.31434913	5.075820199	0.00072	0.05695
mmu-miR-30c-2-3p	53.09431388	144.7153584	2.725628185	0.00142	0.10178
mmu-miR-181b-5p	322.0964351	692.1797756	2.148983038	0.00198	0.12856
mmu-miR-132-3p	18.19780033	55.98987347	3.076738533	0.00237	0.13843
mmu-miR-125b-1-3p	57.21390926	149.4144141	2.61150507	0.00252	0.13843
mmu-let-7b-5p	3230.518751	6635.618825	2.054041266	0.00386	0.18699
mmu-let-7c-5p	4882.488078	9682.89278	1.983188208	0.00392	0.18699
mmu-let-7c-5p	4830.155427	9473.284502	1.961279434	0.00454	0.20266
mmu-miR-200b-3p	30.59796659	2.536806286	0.082907676	0.00572	0.23647
mmu-miR-212-5p	22.91091627	62.99404349	2.749520917	0.00624	0.23647
mmu-miR-744-5p	291.9365094	947.0853346	3.244148313	0.00628	0.23647
mmu-let-7d-5p	1811.726444	3458.665196	1.909043834	0.00669	0.23913
mmu-miR-1249-3p	37.47564173	96.24148751	2.568107791	0.00876	0.29838
mmu-let-7a-5p	4387.689636	8066.421029	1.838421059	0.01006	0.31336
mmu-miR-6240	103.1427418	232.1333021	2.250602398	0.01008	0.31336
mmu-let-7a-5p	4333.114144	7889.456427	1.820735888	0.01079	0.32134
mmu-miR-5126	2.696936877	15.75565412	5.842055203	0.01285	0.36122
mmu-let-7f-5p	2713.767599	4856.736179	1.789665475	0.01314	0.36122
mmu-let-7f-5p	2436.096432	4328.468006	1.776804871	0.01463	0.37916
mmu-miR-10a-5p	1161.619985	543.2343346	0.467652366	0.01580	0.37916
mmu-miR-483-3p	1.571038647	11.09386871	7.06148683	0.01621	0.37916
mmu-miR-1940	9.943323837	34.78604993	3.498432768	0.01630	0.37916
mmu-miR-155-5p	23.75533994	56.56196019	2.381020871	0.02125	0.47476
mmu-miR-193b-3p	110.9863584	14.5344591	0.130957167	0.02673	0.56202
mmu-miR-27a-3p	344.6710656	155.8005298	0.452026716	0.02787	0.56935
mmu-miR-223-3p	40.18786432	8.282510982	0.206094828	0.03733	0.74143
mmu-miR-1306-5p	2.978411435	15.05498902	5.054704277	0.04746	0.90606

Online Table IV. List of potential *NSRP1*-targeting transcription factors measured in the sinus node using Taqman Low density array cards. Significant differences highlighted by P values in bold font.

mRNA	Sedentary		Trained		P value
	Mean	SEM	Mean	SEM	
Predicted by MatInspector					
Zfp354c	1.60E-01	2.89E-02	4.20E-01	8.86E-02	**0.008446**
Helt	1.69E-04	6.57E-05	3.53E-03	2.18E-03	**0.010665**
Six3	1.69E-04	6.57E-05	6.07E-02	3.91E-02	**0.016301**
Patz1	2.51E-01	4.44E-02	4.73E-01	5.95E-02	**0.016376**
Mitf	9.03E-01	2.95E-01	1.86E+00	3.39E-01	**0.021262**
Cdx2	1.69E-04	6.57E-05	1.28E-03	8.71E-04	**0.025429**
Hsf2	2.97E-01	3.66E-02	5.87E-01	1.36E-01	**0.031703**
Pdx1	1.69E-04	6.57E-05	4.37E-04	1.57E-04	**0.034216**
Spz1	1.69E-04	6.57E-05	4.37E-04	1.57E-04	**0.034216**
Foxp1	6.54E-01	6.19E-02	1.11E+00	1.67E-01	**0.035768**
Nkx2.5	1.02E+00	3.55E-01	2.15E+00	3.73E-01	**0.041394**
Tead4	5.68E-02	9.45E-03	9.60E-02	1.04E-02	**0.041491**
Stat3	1.03E+00	1.80E-01	1.80E+00	2.84E-01	**0.042595**
Cebpe	3.34E-02	1.19E-02	4.37E-04	1.57E-04	0.057859
Atf1	2.01E-01	4.19E-02	7.91E-02	1.69E-02	0.058164
Tcf3	3.67E-03	9.86E-04	3.31E-02	2.50E-02	0.061033
Sp1	6.67E-01	9.47E-02	1.07E+00	1.43E-01	0.070278
Hoxa9	6.95E-03	2.10E-03	2.97E-03	7.65E-04	0.074478
Pitx2	9.98E-02	1.13E-02	1.58E-01	2.51E-02	0.093084
Arid5a	8.09E-02	7.66E-03	1.27E-01	2.14E-02	0.103987
Sall2	2.16E-04	7.01E-05	4.37E-04	1.57E-04	0.104569
Klf15	1.39E+00	2.82E-01	3.36E+00	1.12E+00	0.114708
Nanog	4.90E-03	2.87E-03	1.70E-03	1.20E-03	0.123074
Zfp217	7.52E-02	1.53E-02	1.21E-01	2.19E-02	0.142784
Gabpa	3.06E+00	3.75E-01	5.13E+00	1.27E+00	0.149457
Hic1	4.06E-03	2.24E-03	1.32E-01	1.28E-01	0.158815
Tfap2a	2.13E-02	3.54E-03	3.78E-02	1.06E-02	0.162104
Lef1	4.28E-03	7.25E-04	1.08E-02	3.32E-03	0.162278
Klf7	4.21E-01	2.78E-01	1.07E-01	2.15E-02	0.166922
Esrra	5.99E-01	6.75E-02	8.59E-01	1.37E-01	0.185812
Nfatc2	1.41E-01	3.01E-02	2.49E-01	8.32E-02	0.216844
Arid1a	8.23E-02	1.68E-02	5.63E-02	5.22E-03	0.233172
Zfp384	1.29E-01	2.37E-02	1.03E-01	2.55E-02	0.241921
Yy1	5.11E-01	4.11E-02	7.03E-01	1.18E-01	0.302407
Atf6	5.64E-01	5.84E-02	5.72E-01	1.53E-01	0.306556
Gata1	7.68E-03	2.41E-03	6.18E-03	2.94E-03	0.323467
Csrnp3	1.51E-02	5.26E-03	9.08E-03	1.86E-03	0.331801
Grhl2	2.61E-02	2.37E-02	6.46E-02	4.41E-02	0.349373
Pou2f1	8.36E-01	1.77E-01	1.28E+00	3.66E-01	0.362792
Runx3	2.83E-02	7.21E-03	2.52E-02	1.41E-02	0.407731
Satb1	4.42E-01	7.15E-02	5.67E-01	1.04E-01	0.421099

Online Table IV (continued).

mRNA	Sedentary		Trained		
	Mean	SEM	Mean	SEM	P value
Predicted by MatInspector					
Pou4f3	6.39E-02	6.38E-02	1.52E-02	1.47E-02	0.422668
Pou1f1	1.23E-02	1.19E-02	4.67E-02	4.63E-02	0.446538
Zfx	2.05E-02	4.25E-03	2.44E-02	6.31E-03	0.466673
Irx3	7.73E-02	4.40E-02	3.64E-02	1.79E-02	0.478955
LIZfp239	7.25E-02	1.13E-02	7.32E-02	1.46E-02	0.503171
Sox6	2.04E-01	1.34E-02	2.25E-01	6.12E-02	0.511482
Mef2c	6.16E-01	7.84E-02	7.85E-01	1.73E-01	0.513938
Isl2	8.31E-02	6.57E-02	7.60E-02	6.64E-02	0.524187
Gfi1	1.09E-02	7.17E-03	1.34E-02	1.30E-02	0.567992
E2f1	2.31E-02	3.63E-03	2.46E-02	6.81E-03	0.580365
Dmtf1	1.30E-01	2.59E-02	1.87E-01	6.50E-02	0.584297
Hnf4a	1.89E-04	7.24E-05	9.13E-04	4.79E-04	0.613491
Insm2	8.87E-03	5.69E-03	5.02E-03	1.88E-03	0.614452
Hmbox1	1.13E-01	2.12E-02	1.22E-01	2.29E-02	0.619181
Zic3	1.82E-02	1.80E-02	1.54E-03	1.09E-03	0.622457
Rfx5	1.45E+00	3.21E-01	5.18E+00	1.54E+00	0.645909
Pax4	4.94E-02	3.88E-02	4.27E-02	3.84E-02	0.666232
Hltf	3.42E-01	3.49E-02	3.79E-01	5.85E-02	0.717274
Irf3	2.71E-01	1.00E-01	2.36E-01	3.23E-02	0.728975
Six2	1.53E-02	5.42E-03	1.46E-02	3.05E-03	0.732889
Plag1	5.90E-02	9.81E-03	5.97E-02	2.17E-02	0.739622
Zscan21	1.01E-01	2.23E-02	2.22E-01	5.05E-02	0.747869
Sall1	9.02E-03	2.60E-03	6.42E-03	1.73E-03	0.760965
Zbtb14	4.58E-02	8.27E-03	5.04E-02	1.18E-02	0.771122
Pax6	1.30E-01	1.29E-01	4.37E-04	1.57E-04	0.772495
Gli3	5.13E-02	1.11E-02	5.93E-02	1.35E-02	0.772616
Klf4	1.84E+00	4.39E-01	1.40E+00	4.12E-01	0.778102
Nr5a2	4.22E-03	1.57E-03	4.22E-03	1.96E-03	0.778849
Mzf1	7.69E-03	2.79E-03	6.75E-03	1.25E-03	0.811114
Nfkb2	2.56E-01	7.79E-02	2.67E-01	8.14E-02	0.857029
Foxh1	3.41E-02	2.78E-02	7.94E-03	5.42E-03	0.858473
Ikzf5	3.30E-01	6.57E-02	3.22E-01	3.27E-02	0.86262
Prrx2	1.81E-02	2.51E-03	3.21E-02	1.17E-02	0.863999
Smad3	2.20E-01	7.46E-02	2.23E-01	6.69E-02	0.870408
Rbpj	3.49E-01	1.26E-01	2.82E-01	4.66E-02	0.950006
Nfe2l1	8.02E-01	1.40E-01	7.90E-01	2.03E-01	0.950954
Zfp410	3.67E-01	7.91E-02	3.85E-01	8.60E-02	0.956282
Myt1l	3.75E-03	1.43E-03	3.97E-03	2.66E-03	0.992775

Online Table IV (continued).

mRNA	Sedentary		Trained		
	Mean	SEM	Mean	SEM	P value
Predicted by MatInspector					
Known regulators of cardiac function/development					
Tbx5	4.02E+00	9.96E-01	9.43E+00	1.73E+00	**0.013147**
Rest	2.25E-01	4.29E-02	5.24E-01	1.43E-01	**0.040982**
Hand2	1.92E+00	6.53E-01	3.61E+00	7.98E-01	0.076046
Tbx18	4.11E-01	1.06E-01	5.65E-01	1.05E-01	0.204897
Gata4	1.43E+00	2.54E-01	1.79E+00	2.09E-01	0.299239
Isl1	1.91E-01	5.82E-02	1.14E-01	2.35E-02	0.304207
Shox2	7.02E-02	2.42E-02	7.02E-02	1.20E-02	0.451147
Stat5a	3.04E-01	9.58E-02	3.27E-01	4.78E-02	0.454078
Tbx3	4.43E-01	1.75E-01	3.00E-01	5.70E-02	0.955335
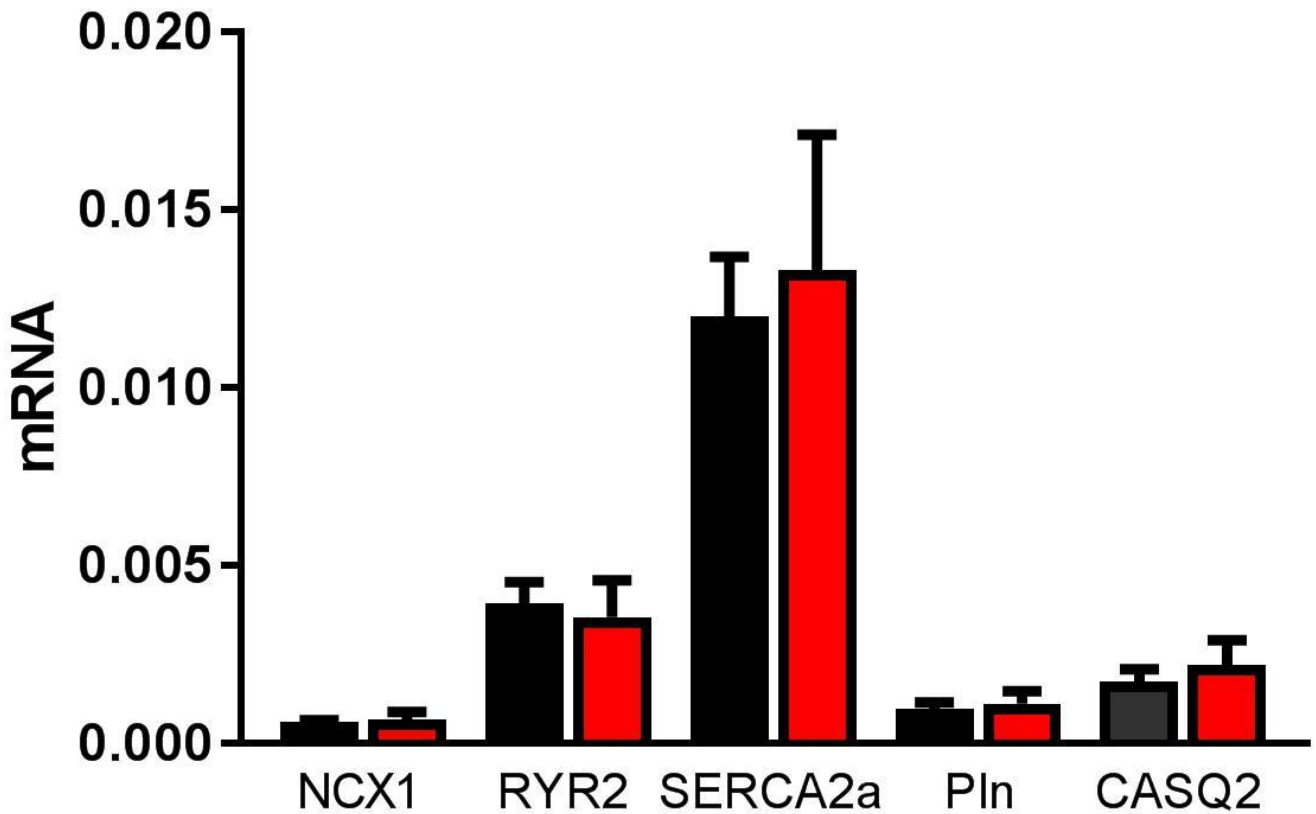
Online Figure I. mRNA expression levels for key proteins involved in the Ca^{2+} clock pacemaker mechanism in sinus node of sedentary (black bars) and trained (red bars) mice (n=5/5).



```
157   CTGCCCTCGCCCTCT--CCCTCG   CDR
      |||||  |||||    ||||||:
      TTTCAGAGCGAGAGACGGGGAGT
1036  TTCATCTC-CTCCATCCCTGTCG   CDR
      ||||  |||   |  ||:  ||:
      TTTCAGAGCGAGAGACGGGGAGT
1602  GGAG-C-AGTAC-ATGTCCTTCC   CDR
      ::||  |   |:  |   ||:||:||
      TTTCAGAGCGAGAGACGGGGAGT
2519  CTTCACCCGCCAGCAGCCCCTCA   CDR
      |||     |  |||||||||
      TTTCAGAGCGAGAGACGGGGAGT
2584  CTGG-CTGGATTCTCTGCACCTCC  CDR
      :|  ||  |  :|||||||| ||||
      TTTCAGAGC-GAGAGACGGGGAGT
3307  AGGGCCTCGC-CTC-ACTCCTCA   CDR
      |::|  ||||||  |||   |:|||||
      TTTCAGAGCGAGAGACGGGGAGT
3604  TGAG-CTGGGCCCTCCCTCCCTCT  3'-UTR
      :||  ||  |  |  |||   :|||||
      TTTCAGAGC-GAGAGACGGGGAGT
3633  TCTTGCTC-CTTTCT-TCCTTCA   3'-UTR
      |||  ||:|||  :||:||| ||
      TTTCAGAGCGAGAGACGGGGAGT
```

**Online Figure II. miR-423-5p binding sites on HCN4 exons (CDR, coding regions) and 3′-UTR predicted by RNA22.**
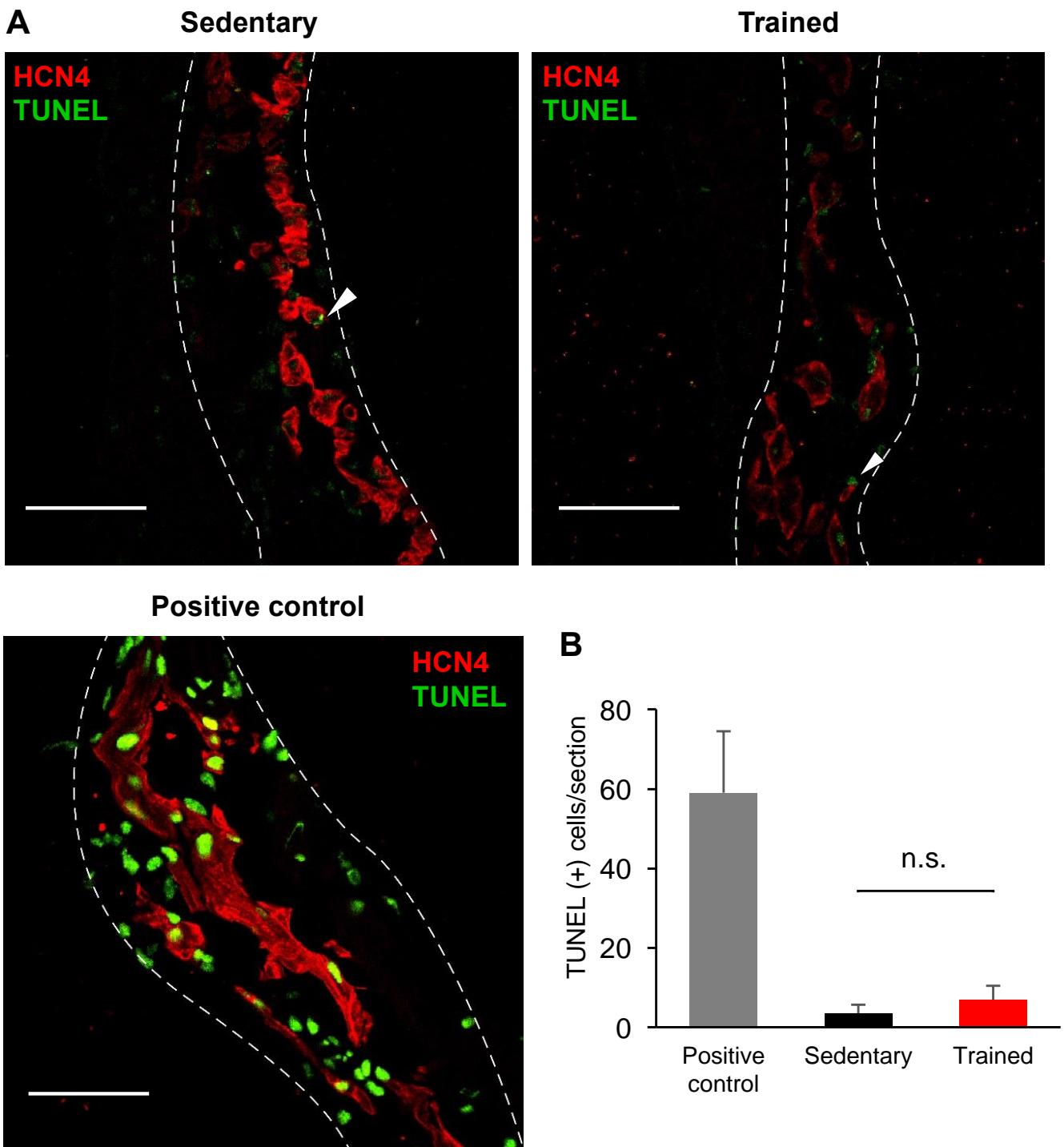
Online Figure III. TUNEL-staining of apoptotic cells in the sinus node of sedentary and trained mice. A, Sections through the sinus node treated with TUNEL (green signal; marker for apoptotic cells) and immunolabelled for HCN4 (red signal; marker for sinus node cells). Sections through the sinus node of sedentary and trained mice shown. A section though the sinus node treated with micrococcal nuclease (triggers apoptosis) also shown as a positive control. Arrowheads indicate TUNEL-positive cells. Scale bars=50 μm. **B**, Average number of TUNEL-positive cells in micrococcal nuclease-treated sinus node sections (positive control) and sinus node sections from sedentary and trained mice. (n=5/5) There were only a few apoptotic cells in the sinus node of sedentary and trained mice (3.48±2.16 versus 6.92±3.48 cells/section; P=0.4297) in contrast to the micrococcal nuclease-treated sinus node sections (59.0±15.5; P=0.001). n.s., not significant.
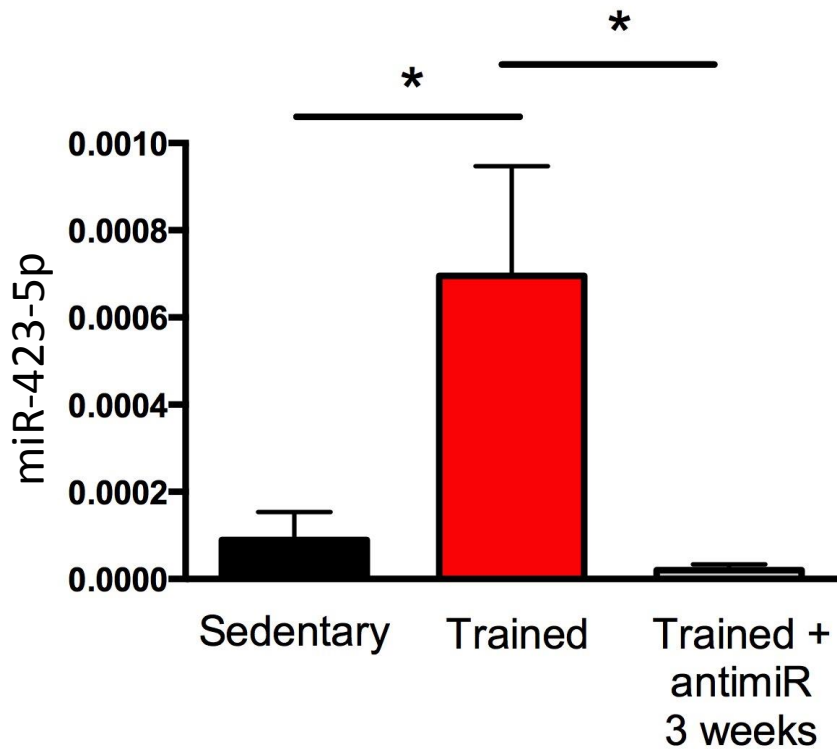
Online Figure IV. Effect of antimiR in trained animals after three weeks. miR-423-5p mRNA (normalised to RNU1A1) determined by qPCR in vehicle-injected sedentary mice, vehicle-injected trained mice and antimiR-injected trained mice three weeks after the last injection of the vehicle or antimiR (*n*=6/5/5). During this additional 3-week period, training of the mice continued. *significantly different (P<0.05).
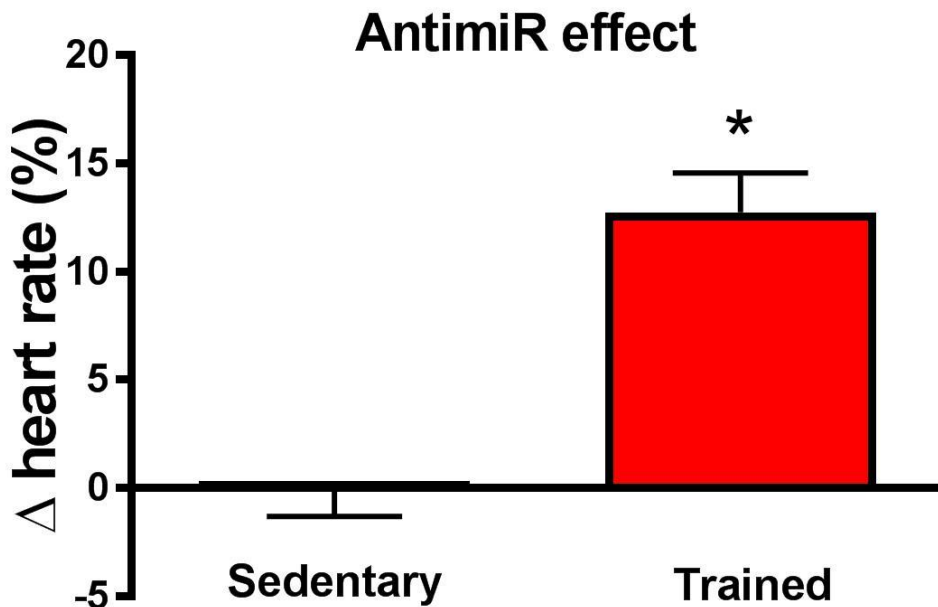
Online Figure V. Effect of antimiR on the heart rate in conscious sedentary and conscious trained mice (n=5/12). The change in heart rate caused by the antimiR is shown (calculated as the difference in heart rate, measured in the conscious mouse, before and 24 h after the third antimiR injection (day 28 of swim training). *significantly different from sedentary data (P<0.05).
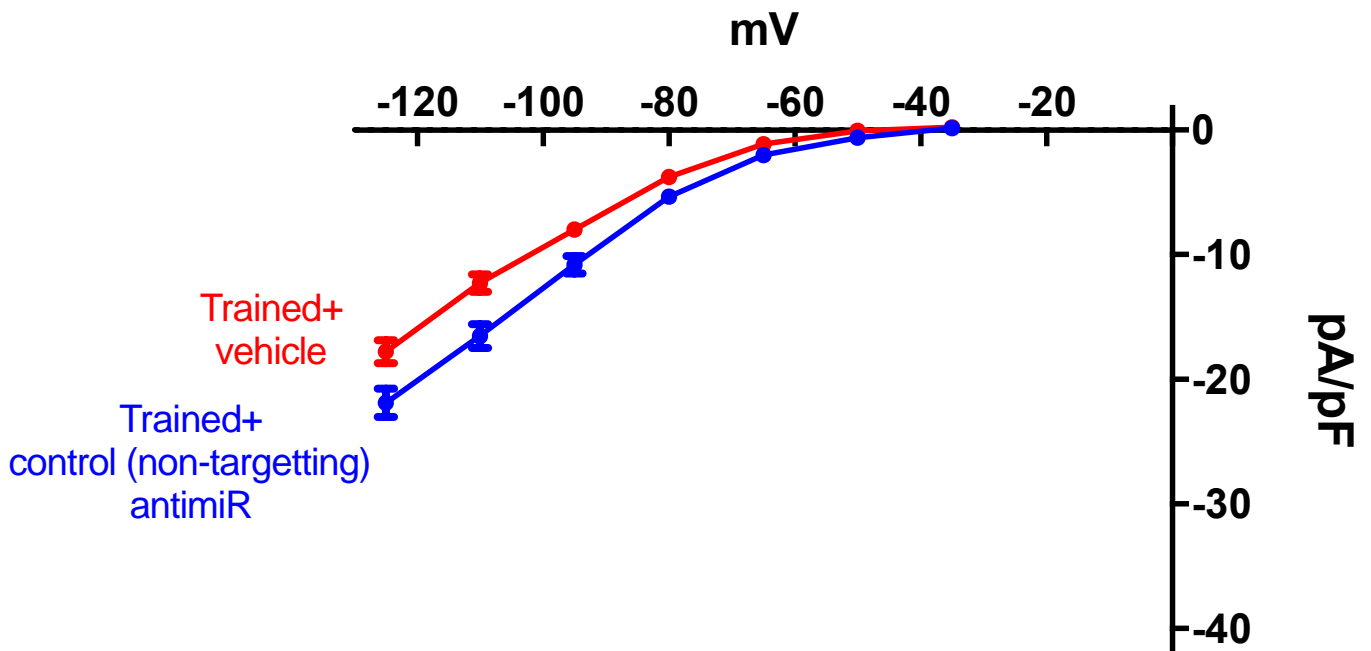
Online Figure VI. A control (non-targeting) antimiR has little effect on I_f in trained mice. Mean current-voltage relationships for I_f from vehicle-treated trained (n=47 cells/5 animals) and control (non-targeting) antimiR-treated trained (n=37 cells/4 animals) mice.
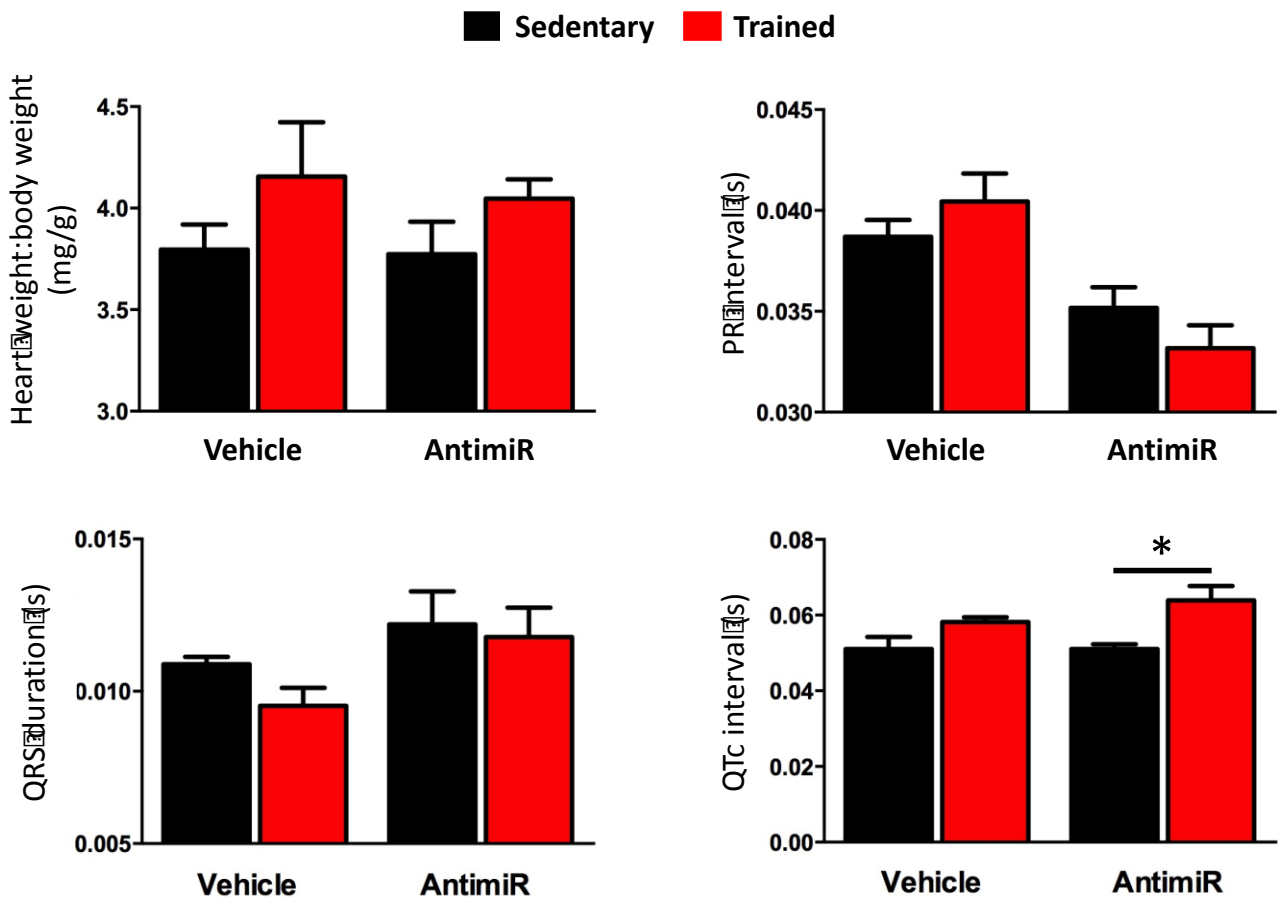
Online Figure VII. The antimiR has little or no effect on heart weight:body weight ratio, PR interval, QRS duration and QTc interval of sedentary or trained mice. n=5/5/5/6 for heart weight:body weight ratio. ECG parameters measured under isofluorane anaesthesia. Continuous 100 beat recordings were analysed and averaged. n=10/10/5/11 for ECG parameters. *significantly different (P<0.05).

	Mouse NSRP1; Chromosome 11
Nkx2.5 binding sites	77080375- ATAAATAATTGTTTAAAAA (1/0.88)
	77079441- GTGTCTGAGTGGTTTGTAC (1/0.99)

Online Figure VIII. Nkx2.5 binding sites in 2 kb 5' flanking region of the miR-423 host gene NSRP1 predicted by MatInspector. Numbers before sequences represent the position of the binding sites in the genome. Numbers in brackets indicate similarity scores for predicted Nkx2.5 binding motifs to canonical core binding sites and overall matrix for Nkx2.5 action respectively.
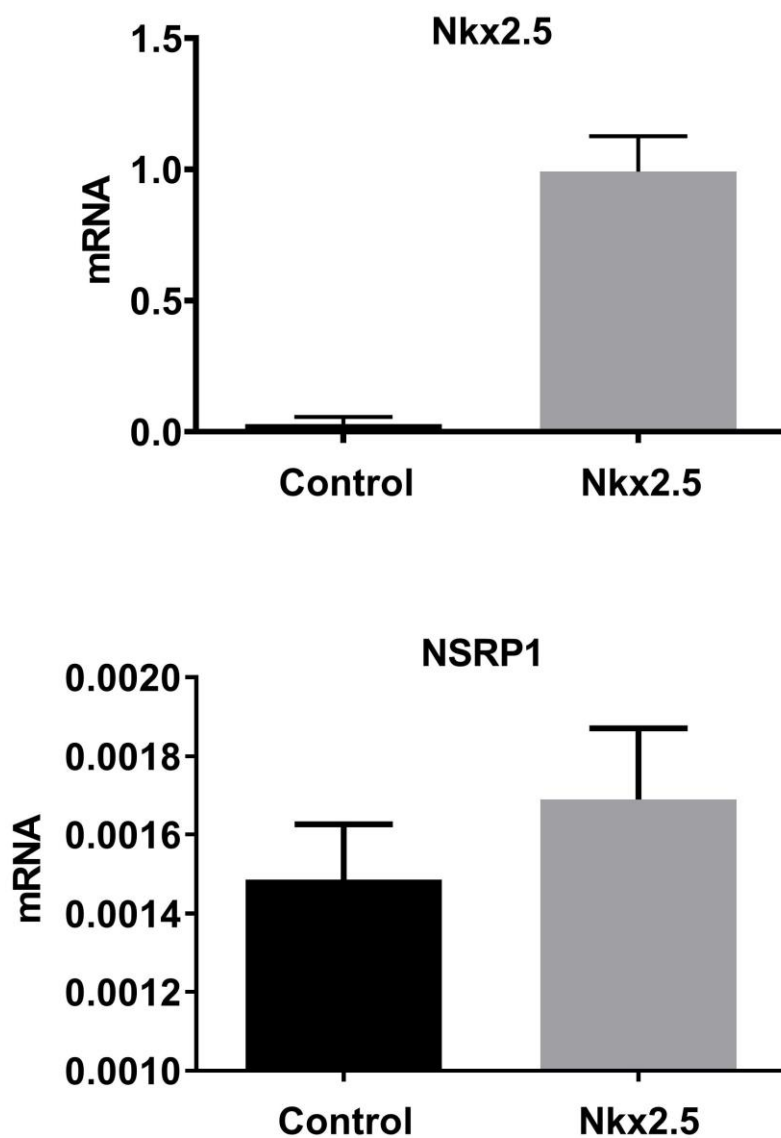
Online Figure IX. Effect of overexpression of Nkx2.5 on mRNA levels of Nkx2.5 and NSRP1 in H9c2 cells. Expression is shown in vehicle-transfected cells (control) or cells transfected with Nkx2.5.
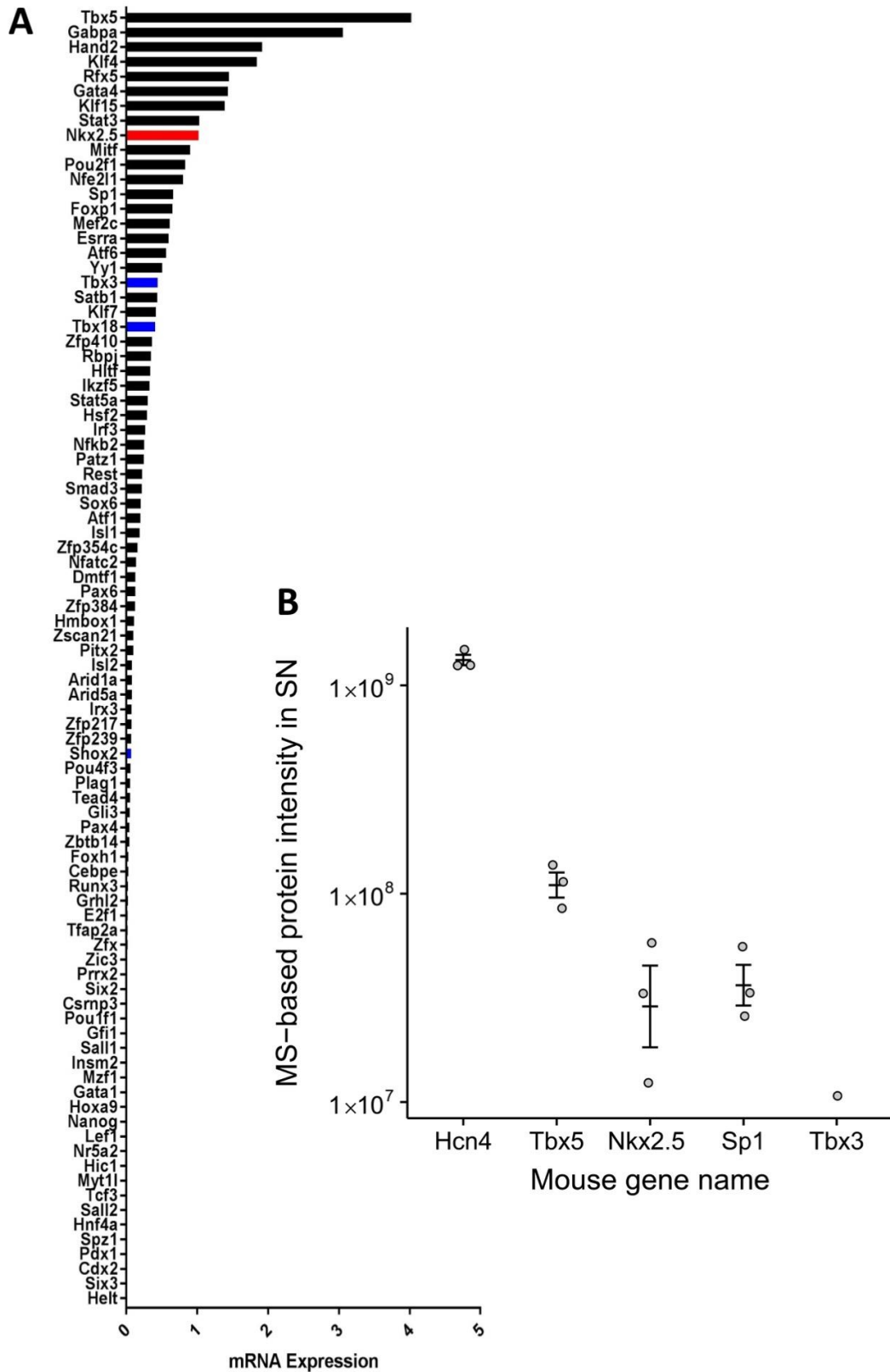
Online Figure X. Expression of Nkx2.5 in the sedentary adult mouse sinus node. A, mRNA expression level of 88 transcription factors in the sedentary adult mouse sinus node (n=8) measured using Taqman low density array cards and normalised to expression level of housekeeping genes GAPDH and TBP. Nkx2.5 is highlighted in red and, for comparison, Tbx3, Tbx18 and Shox2 are highlighted in blue. **B**, Protein expression level (on logarithmic scale) of selected transcription factors, including Nkx2.5, in the sedentary adult mouse sinus node (n=3 cohorts of 10 mice) measured using high-resolution mass spectrometry. Protein expression level of HCN4 also shown. Indivdual data points (for the three cohorts of mice) as well as means±SEM shown. MS, mass spectrometry. SN, sinus node.